A Comprehensive Mass Flux Scheme for Cumulus Parameterization in Large-Scale Models

M. TIEDTKE

ECMWF, Reading, England

(Manuscript received 23 February 1988, in final form 28 February 1989)

ABSTRACT

Observational studies indicate that a mass flux approach may provide a realistic framework for cumulus parameterization in large-scale models, but this approach, through the introduction of a spectral cloud ensemble, leads normally to rather complex schemes. In this paper the question is addressed whether much simpler schemes can already provide realistic values of the thermal forcing by convection under various synoptic conditions. This is done through verifying such a scheme first on data from field experiments for periods of tropical penetrative convection (GATE, Marshall Islands), tradewind cumuli (ATEX, BOMEX) and extratropical organized convection (SESAME-79) and then in a NWP model.

The scheme considers a population of clouds where the cloud ensemble is described by a one-dimensional bulk model as earlier applied by Yanai et al. in a diagnostic study of tropical convection. Cumulus scale downdrafts are included. Various types of convection are represented, i.e., penetrative convection in connection with large-scale convergent flow, shallow convection in suppressed conditions like tradewind cumuli and midlevel convection like extratropical organized convection associated with potentially unstable air above the boundary layer and large-scale ascent. The closure assumptions for determining the bulk cloud mass flux are: penetrative convection and midlevel convection are maintained by large-scale moisture convergence and shallow convection by supply of moisture due to surface evaporation.

The parameterization produces realistic fields of convective heating and appears to be in fair balance with real data for NWP as it does not initiate strong adjustment processes (spinup) in global forecasts.

1. Introduction

Cumulus convection plays a key role in determining the vertical structure of temperature and moisture fields of the atmosphere and therefore must be adequately represented in large-scale models as used for general circulation studies and weather forecasting. Since these models resolve only scales which are much larger than the cumulus scale, however, it is only possible to represent the collective effects of cumulus clouds by means of parameterization. Various methods are presently applied for this purpose in numerical models such as the Kuo-scheme at ECMWF and NMC and a mass flux approach at the meteorological services in France and England. Cumulus parameterization, though generally considered important for the simulation of the large-scale flow in particular in tropical regions, is still rather uncertain and may largely contribute to forecast errors. Some progress has recently been made at ECMWF in cumulus parameterization which lead to significant improvements in tropical forecasts (Tiedtke et al. 1988), but ECMWF operational forecasts still exhibit large deficiencies in the simulated large-scale flow that point strongly towards further deficiencies in cumulus parameterization. Most noticeable is the collapse, within a few days, of the Hadley circulation over the Indonesian area accompanied by a lack of penetrative cumulus convection in the area and the evolution of large errors in the zonal mean flow in the upper troposphere in the tropics. Therefore the problem of cumulus parameterization is being reconsidered at ECMWF by addressing some basic questions as to the design of a practical scheme for large-scale models. The demands on such a scheme are great as the scheme must accurately represent various types of convection occurring over the globe. We take the view that for this purpose it is best to follow closely observational studies on convection which, over the last 25 years, have contributed much to our understanding of cumulus convection and its effects on the large-scale fields of temperature and moisture.

Real-data diagnostic studies carried out for periods of tropical convection (e.g., Yanai et al. 1973; Ogura and Cho 1973; Nitta 1978; Johnson 1976, 1980; Chen 1985; review article by Houze and Betts 1981 on convection during GATE) and for tradewind cumulus convection (e.g., Nitta 1975) have shown that in order to reproduce the contributions from convection to the large-scale apparent heat and moisture sources it is sufficient to describe the cloud population by a highly

Corresponding author address: Dr. Michael Tiedtke, ECMWF, Shinfield Park, Reading, Berkshire RG2 9AX, England.

idealized ensemble of clouds, where the clouds are represented by simple prototypes of one-dimensional entraining plumes. The cumulus ensemble consists of clouds of various sizes (spectral cloud ensemble), but recent studies indicate that besides cumulus-scale updrafts, cumulus-scale downdrafts and the organization of penetrative cells in mesoscale cloud clusters and squall lines with well-developed mesoscale circulations on their own can also be important for the large-scale heat and moisture budgets (see review article by Houze and Betts 1981). In the parameterization presented here, we apply the same simple concept of cumulus clouds, considering cumulus scale updrafts as well as downdrafts; but mesoscale circulations are neglected as there is presently little understanding of how to parameterize them.

The evolution of cloud ensembles in relation to the synoptic flow is not well understood and therefore reliable parameterization rules are not available. Here we investigate the possibility of the simplest approach where the cloud ensemble is not explicitly resolved but is represented as a bulk by means of a bulk model. In representing the cloud ensemble in this way we follow an earlier diagnostic study by Yanai et al. (1973) who prior to the introduction of spectral cloud ensembles in diagnostic studies applied a bulk model and obtained realistic contributions from convection to the large-scale budgets of heat and moisture. However, whereas Yanai et al. derived cloud bulk values to reproduce the apparent heat source and moisture sink, in a parameterization cloud properties have to be specified through closure assumptions which is the most difficult and most uncertain part of the parameterization. The closure of this scheme is based on the observational evidence that typical cloud ensembles prevail under certain synoptic conditions; for example, penetrative convection frequently occurs in connection with strong low-level convergent flow, whereas shallow cumuli are predominant in suppressed conditions such as during periods of undisturbed trades. We shall make convection dependent on the moisture supply by large-scale flow convergence and boundary layer turbulence, which makes it a closure of type IV in the sense of Arakawa and Chen (1987). Details about cloud model and closure assumptions are given in section 3.

Diagnostic studies have been mainly concerned with tropical convection and tradewind cumuli but less with extratropical convection. From the viewpoint of parameterization extratropical convection, which is different from tropical convection, is particularly significant and needs special consideration in a parameterization designed for global models. An important example is convection that occurs in rainbands at the warm front and in the warm sector of extratropical cyclones (e.g., Browning et al. 1973; Houze et al. 1976; review article by Houze and Hobbs 1982). This type of convection differs from tropical convection as it is associated with the lifting of a potentially unstable layer of upper air rather than near surface air. A parameterization for midlevel convection is presented in section 3e.

A particular problem with the mass flux approach arises from the discretization of the transport terms and in the large-scale budget equations as it strongly affects the vertical profiles of convective heating and moistening. This is discussed in section 4. The scheme is verified on real data for periods of penetrative convection during GATE and over the West Pacific, for tradewind convection during ATEX and BOMEX, and for extratropical organized convection during SESAME-79, the results are summarized in section 5. In section 6 results from global forecasts are presented and section 7 contains a general discussion and conclusions.

2. Large-scale budget equations

Because we are only concerned here with the thermodynamic forcing by cumulus convection, we apply the large-scale equations for heat and moisture as

$$\frac{\partial \bar{s}}{\partial t} + \bar{\mathbf{v}} \cdot \nabla \bar{s} + \bar{w} \frac{\partial \bar{s}}{\partial z} = -\frac{1}{\bar{\rho}} \frac{\partial}{\partial z} (\bar{\rho} \overline{w's'}) + L(\bar{c} - \bar{e}) + \overline{Q_R} \quad (1)$$

$$\frac{\partial \bar{q}}{\partial t} + \bar{\mathbf{v}} \cdot \nabla \bar{q} + \bar{w} \frac{\partial \bar{q}}{\partial z} = -\frac{1}{\bar{\rho}} \frac{\partial}{\partial z} (\bar{\rho} \overline{w'q'}) - (\bar{c} - \bar{e}), \quad (2)$$

where $s = C_pT + gz$ is the dry static energy, q the specific humidity, ρ the density of air, v the horizontal velocity, w the vertical velocity, c the rate of condensation, e the rate of evaporation and Q_R the radiative heating. The overbar denotes averages over a horizontal area that is large enough to contain an ensemble of cumulus clouds, and the prime denotes deviations from the horizontal average. The vertical eddy fluxes of dry static energy and moisture comprise many scales, but here we consider only the convective scale, assuming that the parameterization of boundary layer turbulence, for example, can be done separately. Also, mesoscale circulations are ignored. The horizontal eddy flux divergences of s and q are neglected as the net lateral horizontal transports across the boundary of a large-scale area by cumulus convection are small in comparison to the transports by the large-scale flow.

The eddy transports of dry static energy s and moisture q contain contributions from cumulus updrafts, cumulus downdrafts and the cumulus-induced subsidence in the environmental air as

$$\bar{\rho}(\overline{w's'})_{cu} = \bar{\rho} \sum_i a_{ui}(w_{ui} - \bar{w})(s_{ui} - \bar{s}) + \bar{\rho} \sum_i a_{di}(w_{di} - \bar{w})(s_{di} - \bar{s}) + \bar{\rho}\left[1 - \sum_i (a_{ui} + a_{di})\right](\tilde{w} - \bar{w})(\tilde{s} - \bar{s}), \quad (3)$$

and similarly for moisture. The subscript *cu* denotes the contribution from cumulus convection, *i* denotes cloud type *i*, *u* and *d* denote cumulus updrafts and downdrafts, tilde the environmental air, and *a* is the fractional area coverage. The contributions from updrafts, downdrafts and environmental subsidence have already been expressed using average values, as we assume that the convective updrafts and downdrafts can be adequately modeled by one-dimensional models. For the purpose of cumulus parameterization in large-scale models the approximation $\tilde{s} = \bar{s}$, $\tilde{q} = \bar{q}$ is well justified. Also, it is convenient to introduce convective mass fluxes:

$$M_{ui} = \bar{\rho} a_{ui}(w_{ui} - \bar{w}), \quad M_{di} = \bar{\rho} a_{di}(w_{di} - \bar{w}), \quad (4)$$

M_{ui} and M_{di} being the updraft mass flux and downdraft mass flux for cloud type *i*, respectively.

As already mentioned, we do not describe the single components of the cloud ensemble but only their bulk properties by means of a bulk model similar to that used in earlier studies of tropical convection (Yanai et al. 1973, 1976; Reed and Johnson 1974). Then the large-scale budget equations (1) and (2) become

$$\frac{\partial \bar{s}}{\partial t} + \bar{\mathbf{v}} \cdot \nabla \bar{s} + \bar{w} \frac{\partial \bar{s}}{\partial z} = -\frac{1}{\bar{\rho}} \frac{\partial}{\partial z} [M_u s_u + M_d s_d - (M_u + M_d)\bar{s}] + L(c_u - e_d - \tilde{e}_l - \tilde{e}_p) - \frac{1}{\bar{\rho}} \frac{\partial}{\partial z} (\bar{\rho} \overline{w's'})_{\mathrm{tu}} + \overline{Q_R} \quad (5)$$

$$\frac{\partial \bar{q}}{\partial t} + \bar{\mathbf{v}} \cdot \nabla \bar{q} + \bar{w} \frac{\partial \bar{q}}{\partial z} = -\frac{1}{\bar{\rho}} \frac{\partial}{\partial z} [M_u q_u + M_d q_d - (M_u + M_d)\bar{q}] - (c_u - e_d - \tilde{e}_l - \tilde{e}_p) - \frac{1}{\bar{\rho}} \frac{\partial}{\partial z} (\bar{\rho} \overline{w'q'})_{\mathrm{tu}}, \quad (6)$$

where M_u, M_d, c_u and e_d are the net contributions from all clouds to the upward mass flux, downward mass flux, condensation and evaporation, respectively, and s_u, s_d, q_u and q_d are the weighted averages of s and q from all updrafts and downdrafts. Here $\tilde{e}_l$ is the evaporation of cloud air that has been detrained into the environment and $\tilde{e}_p$ is the evaporation of precipitation in the unsaturated subcloud layer. The index tu denotes boundary layer turbulence. In addition to (5) and (6) we consider the mass continuity equation for rain water as

$$P(z) = \int_z^\infty (G_p - e_d - \tilde{e}_p)\bar{\rho} dz, \quad (7)$$

where $P(z)$ is the rain water flux at height z and G_p is the conversion from cloud water into precipitation.

We note that we shall calculate the contributions from convection to the large-scale budgets of heat and moisture as given by (5) and (6) as convection offers several advantages over the advective form often used:

(i) a guarantee that the total energy is conserved after discretization of the equations;

(ii) numerically consistent calculations of cloud model equations and large-scale budget equations, whereby numerical errors are reduced (see section 4);

(iii) a convenient framework to express the interaction between cloud layer and subcloud layer since cloud base heat and moisture fluxes are readily available;

(iv) realistic thermal forcing is maintained as the model resolution is increased approaching the explicit condensation scheme in case of grid-scale saturated moist adiabatic ascents noting that the bulk of cumulus updrafts follows closely the grid-scale ascent. This is because the convective heating and drying in (5) and (6), respectively, are in this case represented entirely by the condensational terms in the updrafts.

3. The cloud model

The conceptual idea of the cumulus clouds forming the cloud population is that adopted in many diagnostic studies. Cumulus clouds are assumed to be embedded in the large-scale environment, have a common cloud base but different heights of tops due to different sizes with different entrainment and detrainment rates. They are defined by upward and downdraft mass flux and by their thermal properties as dry static energy, moisture and cloud water content.

Observational studies show that the cloud populations consist of a spectrum of clouds and various sizes which largely varies with the synoptic conditions. Parameterization schemes must account for the large-scale thermodynamic and dynamic effects of the total cloud ensembles, but it is not clear how detailed the cloud ensembles must be modeled in a parameterization scheme for large-scale models in order to obtain realistic results; in particular it is presently uncertain whether the single components of the cloud spectrum must be described or a bulk representation is sufficient. Some evidence that a bulk model may be adequate for tropical convection has been provided by Yanai et al. (1976) who show that a bulk model and a spectral model give nearly identical total vertical cloud mass flux, but little is known about cloud populations in other synoptic situations (e.g., midlevel convection in extra tropics). Here we employ a bulk model which is applied separately to cumulus updrafts and cumulus downdrafts with bulk properties [i.e., cloud base mass flux and entrainment/detrainment rates] specified differently for the various types of convection.

a. Cumulus updrafts

The updraft of the cloud ensemble is assumed to be in a steady state. Then the bulk equations for mass, heat, moisture and cloud water content are

$$\left.\begin{aligned}
\frac{\partial M_u}{\partial z} &= E_u - D_u \\
\frac{\partial (M_u s_u)}{\partial z} &= E_u \bar{s} - D_u s_u + L\bar{\rho} c_u \\
\frac{\partial (M_u q_u)}{\partial z} &= E_u \bar{q} - D_u q_u - \bar{\rho} c_u \\
\frac{\partial (M_u l)}{\partial z} &= -D_u l + \bar{\rho} c_u - \bar{\rho} G_p
\end{aligned}\right\}, \quad (8)$$

where E and D are the rates of mass entrainment and detrainment per unit length, l is the cloud liquid water content, and c_u the net condensation in the updrafts. Cloud air is assumed to be saturated and cloud processes are crudely represented. Freezing and melting processes are not considered and the conversion from cloud droplets to raindrops is assumed to be proportional to the liquid cloud water content as

$$G_p = K(z) l, \quad (9)$$

where $K(z)$ is an empirical function that varies with height. This simple parameterization yields rather reasonable vertical distributions of the generation of raindrops (Yanai et al. 1973). Here K is assumed to be zero near cloud base and constant at higher levels:

$$K(z) = \begin{cases} 0, & \text{if } z \leqslant Z_B + 1500 \text{ m} \\ 2.10^{-3} \text{ sec}^{-1}, & \text{if } z > Z_B + 1500 \text{ m}. \end{cases} \quad (10)$$

The choice of $K = 0$ at lower levels ensures that shallow cumuli do not produce precipitation, noting that a sizable portion of the liquid water content in nonprecipitating cumuli is of precipitation-sized drops.

We further note that the cloud liquid water detrained into the environmental air is assumed to evaporate there instantaneously; then

$$\tilde{e}_l = \frac{1}{\bar{\rho}} D_u l. \quad (11)$$

The vertical integration of (8) requires the knowledge of cloud base mass flux and mass entrainment and detrainment. Cloud-base mass flux is determined for the various types of convection from the parameterization assumptions discussed below. Entrainment of mass into convective plumes is assumed to occur through (i) turbulence exchange of mass through cloud edges and (ii) through organized inflow associated with large-scale convergence, detrainment through turbulent exchange and as organized outflow at cloud top:

$$E_u = E_u^{(1)} + E_u^{(2)}, \quad D_u = D_u^{(1)} + D_u^{(2)}. \quad (12)$$

Turbulent entrainment and detrainment are parameterized following Turner (1963) as

$$E_u^{(1)} = \epsilon_u M_u, \quad D_u^{(1)} = \delta_u M_u, \quad (13)$$

where the fractional entrainment/detrainment rates depend inversely on cloud radii (Simpson and Wiggert 1969; Simpson 1971):

$$\epsilon_u = \frac{0.2}{R_u}, \quad \delta_u = \frac{0.2}{R_u}. \quad (14)$$

By assuming typical cloud sizes for the various types of convection, average values of entrainment/detrainment rates are defined: in the presence of synoptic scale flow convergence, large clouds which contribute most to the convective heating and moistening are assumed to exist and consequently small values for the entrainment/detrainment rates are imposed whereas in the absence of flow convergence clouds of smaller sizes with larger entrainment rates prevail. In order to keep the scheme simple we use fixed values of the turbulent entrainment/detrainment rates for each of the various types of convection:

$$\epsilon_u = \delta_u = \begin{cases} 1 \times 10^{-4} \text{ m}^{-1}, & \text{for penetrative and midlevel convection in the presence of large-scale flow convergence} \\ 3 \times 10^{-4} \text{ m}^{-1}, & \text{for shallow convection in suppressed conditions.} \end{cases} \quad (15)$$

For penetrative convection and midlevel convection we deliberately impose a very small value typical for tropical thunder clouds (Simpson 1971) so as not to inhibit the penetration of clouds to large heights (see section 5a). For shallow convection we use a value typical for the larger trade wind cumuli (Nitta 1975), noting that small clouds with much larger entrainment/detrainment rates which detrain immediately above cloud base are not represented in our parameterization (see section 3d below).

The parameterization of organized entrainment and detrainment is discussed in sections 3c–e.

Below cloud base, the net convective fluxes of heat and moisture due to updraft and compensating subsidence in the environment are assumed to decrease linearly from their values at cloud base towards zero at the surface so as not to alter the vertical structure of the subcloud layer and in particular not its well-mixed character.

b. Cumulus downdrafts

Downdrafts are considered to be associated with convective precipitation from the updrafts and originate from cloud air influenced by the injection of environmental air. Following Fritsch and Chappell (1980) and Foster (1958), the level of free sinking (LFS) is assumed to be the highest model level where a mixture of equal parts of cloud air and saturated

environmental air at wet-bulb temperature becomes negative buoyant with respect to the environmental air. The downdraft mass flux is assumed to be directly proportional to the upward mass flux. Following Johnson (1976, 1980) the mass flux at LFS is specified from the updraft mass flux at cloud base as

$$(M_d)_{\mathrm{LFS}} = \gamma(M_u)_{\mathrm{base}} \quad \text{with} \quad \gamma = -0.2. \quad (16)$$

The coefficient γ is a disposable parameter. The uncertainty in the convective forcing introduced through γ is discussed in section 5a below.

The vertical distribution of the downdraft mass flux, dry static energy and moisture below the LFS is determined by the equations for mass, dry static energy and moisture content as

$$\left.\begin{aligned} \frac{\partial M_d}{\partial z} &= E_d - D_d \\ \frac{\partial (M_d s_d)}{\partial z} &= E_d \bar{s} - D_d s_d + L\bar{\rho} e_d \\ \frac{\partial (M_d q_d)}{\partial z} &= E_d \bar{q} - D_d q_d - \bar{\rho} e_d \end{aligned}\right\} . \quad (17)$$

Entrainment and detrainment in downdrafts are highly uncertain as relevant data are not available. Numerical experiments show, however, that the results are rather insensitive to changes in the entrainment and detrainment rates. The results presented below have been obtained using the same parameterization as for the updrafts with

$$\epsilon_d = \delta_d = 2 \times 10^{-4}\ \mathrm{m}^{-1}. \quad (18)$$

This gives a mass flux which is independent of height and which effectively detrains into the environment in the subcloud layer. We also note that e_d is the evaporation of convective rain to maintain a saturated descent and that the moistening and cooling of the environmental air injected at LFS is also due to evaporating rain. As the downdrafts are determined from the updrafts the remaining parameterization task is to specify the updraft. This is done by means of closures defined below for the various types of convection.

c. *Penetrative convection*

Many diagnostic studies show that penetrative convection predominantly occurs in disturbed situations and strongly depends on low-level synoptic scale convergence. Various parameterization schemes are based on this relationship in one way or another. Here, we apply a moisture convergence hypothesis; following Kuo (1965, 1974) and Lindzen (1981), we postulate that when there is a deep layer of conditional instability and large-scale moisture convergence, cumulus clouds exist that entrain environmental air through their base and through their sides directly proportional to the supply of moisture and detrain cloud air at higher levels.

The injection of mass into the clouds through their base is determined by imposing a moisture balance for the subcloud layer such that the moisture content is maintained in the presence of large-scale transports, turbulent transports and convective transports. Because of (6) this balance may be written as

$$[M_u(q_u - \bar{q}) + M_d(q_d - \bar{q})]_B = -\int_0^B \left(\bar{\mathbf{v}} \cdot \nabla \bar{q} + \bar{w}\frac{\partial \bar{q}}{\partial z} + \frac{1}{\bar{\rho}}\frac{\partial}{\partial z}(\bar{\rho}\overline{w'q'})_{\mathrm{tu}}\right)\bar{\rho} dz, \quad (19)$$

where B denotes the cloud base height defined as the condensation level for surface air. The quasi-steady state assumption for the subcloud layer moisture content (19) is identical to that applied in the Kuo-scheme (Kuo 1965, 1974) except here it is expressed in terms of convective fluxes of moisture. The assumption (19) is well justified over the tropical oceans where the boundary layer moisture content typically changes little with time (Ogura and Cho 1974) but little is known how well it holds in other areas. The vertical distribution of the updraft mass flux above cloud base is determined using similar arguments as for the subcloud layer; that is, we postulate that there is organized entrainment which is directly proportional to the large-scale moisture convergence as

$$E_u^{(2)} = -\frac{\bar{\rho}}{\bar{q}}\left(\bar{\mathbf{v}} \cdot \nabla \bar{q} + \bar{w}\frac{\partial \bar{q}}{\partial z}\right). \quad (20)$$

Organized entrainment is only considered in the lower part of the cloud layer where large-scale convergence is encountered, that is, below the level of strongest vertical ascent. The idea to link the cloud mass flux directly to the large-scale moisture convergence has first been advocated as a parameterization by Lindzen (1981) who indicated that it may provide vertical profiles of mass flux and convective heating in good agreement with observations. The assumption (20) ensures that the vertical distribution of the convective mass flux follows that of the large-scale ascent which is partly supported by diagnostic studies for tropical convection (e.g., Cheng et al. 1980; Johnson 1980). Equation (20) forms, together with the assumption (19), for the cloud base mass flux, the basic closure and as such is crucial for the performance of the parameterization of penetrative convection. The verification of the scheme during periods of tropical convection confirms that the closure provides realistic profiles of convective mass fluxes and convective heating (see section 5a). It is worth noting that the closure originally suggested by Lindzen (1981) has previously been adopted with some success for cumulus parameterization by Geleyn et al. (1982).

In addition to organized entrainment we consider turbulent entrainment and detrainment by (13) and

(15). Turbulent entrainment is again only considered at lower cloud levels. The assumption that entrainment is small at higher levels and therefore can be neglected is partly supported by data (Chen 1985).

Cumulus clouds detrain effectively at levels near to their zero-buoyancy level by means of organized outflow. Therefore, the vertical distribution of the total detrainment from all clouds depends on the spectral cloud distribution. Since spectal cloud distribution is not available, however, organized outflow is assumed to occur only in the model layer which contains the zero-buoyancy level of the deepest clouds. Our detrainment assumption implies a unimodal cloud distribution with large detrainment from the deepest clouds and little detrainment from shallow clouds and medium deep clouds. The large contribution from the very deep clouds is in agreement with observations (see, for example, Yanai et al. 1973 and Ogura and Cho 1973) but the assumption about shallow cumuli is questionable as they are often observed to produce another detrainment maximum immediately above cloud base. The effect from shallow cumuli has been neglected because their parameterization is a still unsolved problem. This is because the role of shallow cumuli in connection with penetrative convection is not well understood, particularly when cumulus downdraft occur simultaneously as these compete with shallow convection having similar effects on the environment as shallow cumuli (Johnson 1976). The results obtained with this scheme indicate, however, that neglecting the contributions from shallow cumuli when penetrative convection is encountered does not introduce large errors in the convective heating and drying.

d. *Shallow convection*

Here we consider cumulus convection, which predominantly occurs in undisturbed flow, that is in the absence of large-scale convergent flow. Typical examples are tradewind cumuli under a subsidence inversion, convection occurring in the ridge region of tropical easterly waves and daytime convection over land. This type of convection seems to be effectively controlled by subcloud layer turbulence. In fact, most of the diagnostic studies carried out for tradewind cumuli show that the net upward moisture flux at cloud base level is nearly equal to the turbulent moisture flux at the surface (Le Mone and Pennell 1976). As this implies a quasi-steady moisture balance, we shall apply the same moisture budget equation (19) as for penetrative convection. The difference, however, is that the moisture supply to cumulus clouds is now largely through surface evaporation as the contributions from large-scale convergence are either small or even negative, such as in the undisturbed trades where dry air is transported downward to lower levels.

Under typical tradewind conditions the vertical distribution of the total convective fluxes above cloud base is dominated by two types of clouds: very small cumuli, which in large numbers detrain immediately above cloud base, and deeper clouds, which detrain just beneath and above the trade inversion. The intrusion of cumulus clouds into the stable layer above the inversion is through overshooting of cumuli above their level of zero-buoyancy (Nitta 1975). Because of the coarse resolution employed in large-scale models, where the vertical gridlength is typically 50 mb to 100 mb, it is difficult to represent these two types. The scheme presented here ignores the effect of very small cumuli but tentatively accounts for the effects of overshooting cumuli, as we assume that a given fraction of the cloud ensemble penetrates into the inversion layer and detrains there into the environment. Thus, cloud air shall only partly detrain into the environment within the model layer that contains the zero-buoyancy level; the remaining fraction shall intrude into the next layer above and detrain there (see next paragraph for vertical discretization):

$$\left.\begin{aligned} D_u^{(2)} &= (1-\beta)(M_u)_{k+\frac{1}{2}}/\Delta z \quad \text{for top layer } k \\ D_u^{(2)} &= \beta(M_u)_{k+\frac{1}{2}}/\Delta z \quad \text{for layer } k-1 \\ \beta &= 0.3 \end{aligned}\right\}. \tag{21}$$

Although this parameterization is very crude, it clearly reproduces more realistic trade inversions than when the effect from overshooting cumuli is ignored ($\beta = 0$), as then the inversion becomes too strong in the simulation and the cloud layer below the inversion too moist (as shown in section 5b below for simulations with the BOMEX and ATEX data). The value 0.3 for the disposable parameter β provides the best results and, because there is no other information available, is adopted here.

e. *Midlevel convection*

Midlevel convection, that is, convective cells which have their roots not in the boundary layer but originate at levels above the boundary layer, often occur in rainbands at warm fronts and in the warm sector of extratropical cyclones (Browning et al. 1973; Houze et al. 1976; Herzegh and Hobbs 1980). These cells are probably formed by the lifting of low level air until it becomes saturated (Wexler and Atlas 1959) and the primary moisture source for the clouds is from low-level large-scale convergence (Houze et al. 1976). Often a low-level temperature inversion exists that inhibits convection from starting freely from the surface; therefore convection seems to be initiated by lifting low-level air dynamically to the level of free convection. This occurs often in convection with mesoscale circulations which might be related to conditionally symmetric instability (Bennets and Hoskins 1979; Bennets

and Sharp 1982) or a wave-CISK mechanism (Emanuel 1982).

Although it is not clear how significant the organization of convection in mesoscale rainbands is for the large-scale flow, a parameterization should ideally account for both convective and mesoscale circulations. Such a parameterization, however, is presently not available and we must therefore rely on simplified schemes. Here we propose a parameterization which in a simple way considers the finding of the diagnostic studies mentioned above. We assume that convection is activated when there is large-scale ascent at lower levels, the environmental air is sufficiently moist, i.e., of relative humidity in excess of 90%, and convectively unstable layer exists above. The free convection level is determined by lifting a parcel of environmental temperature and moisture content,

$$T_u = \bar{T}, \quad q_u = \bar{q} \tag{22}$$

adiabatically, allowing for condensational heating, and then checking for buoyancy. The upwards mass flux is set equal to the vertical mass transport by the large-scale flow at that level:

$$(M_u)_B = \bar{\rho}_B \bar{w}_B, \tag{23}$$

which ensures that the amount of moisture which is vertically advected through cloud base by the large-scale ascent is fully available for generation of convective cells.

In addition to the injection of mass through cloud base, we assume again that cloud air is produced by moisture convergence above cloud base through lateral entrainment in the same way as for penetrative convection as given by (20).

4. Discretization of the model equations

The vertical structure of the model is shown in Fig. 1. The vertical coordinate is either defined in pressure p or, through the hydrostatic equation, in height z. The large-scale temperature $\bar{T}$ and the specific humidity $\bar{q}$ are predicted at full levels (solid lines with integer indices) where the large-scale budget equations (5) and (6) are applied. Updraft variables (M_u, s_u, q_u, l) and downdraft variables (M_d, s_d, q_d) are determined from the cloud model equations (8) and (17) at half levels (dashed lines with half-integer indices). The flux divergence terms in the large-scale budget equations (5) and (6) and in the cloud equations (8) and (17) are approximated by centered finite differences as

$$-\frac{1}{\bar{\rho}}\frac{\partial(Ma)}{\partial z} = g\frac{M_{k+\frac{1}{2}}a_{k+\frac{1}{2}} - M_{k-\frac{1}{2}}a_{k-\frac{1}{2}}}{p_{k+\frac{1}{2}} - p_{k-\frac{1}{2}}}, \tag{24}$$

where M and a represent M_u, M_d, $\bar{s}$, $\bar{q}$, s_u, q_u, s_d, q_d, l accordingly. In order to calculate the downward transports of dry static energy $\bar{s}$ and specific humidity $\bar{q}$ by the net cumulus-induced subsidence $M_u + M_d$, half-level values of $\bar{s}$ and $\bar{q}$ must be determined from their full-level values. Numerical tests performed show that the fluxes are very sensitive to the method chosen.

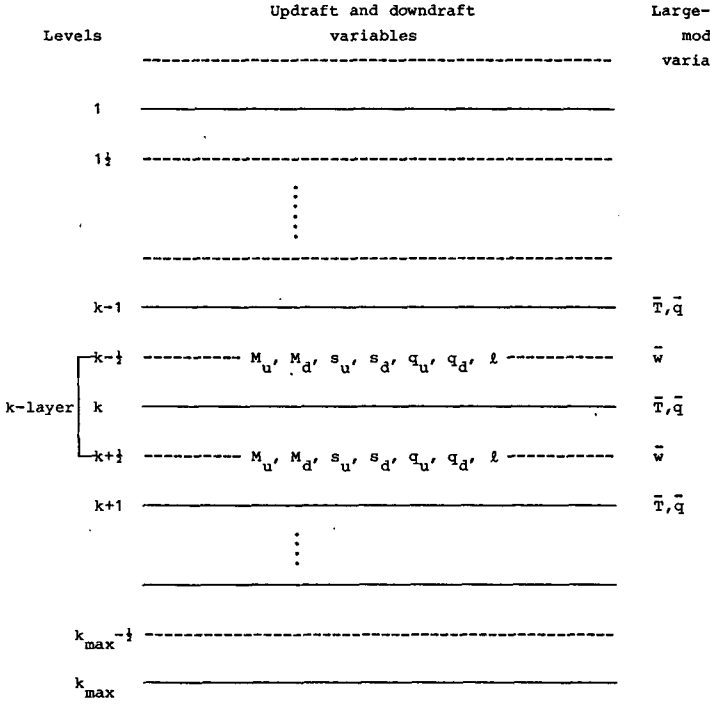

FIG. 1. Vertical structure of the numerical model showing the distribution of model variables on main levels (full lines) and half levels (dashed lines).

This is apparent from Fig. 2, which shows the predicted vertical profiles of temperature and dewpoint for two simulations of the composite easterly wave during GATE (see section 5 below for details of the GATE simulation). When the half-level values are defined by linear interpolation of full-level values [e.g., $\bar{s}_{k+½} = 0.5(\bar{s}_k + \bar{s}_{k+1})$], very noisy profiles evolve in time particularly with regard to humidity. Much smoother profiles are obtained when the half-level values are determined by downward extrapolation from the next full level above along a cloud-ascent through that level:

$$\left.\begin{aligned} \bar{T}_{k+½} &= \bar{T}_k + \left(\frac{\partial T}{\partial p}\right)_{h_{sat}} (p_{k+½} - p_k) \\ \bar{q}_{k+½} &= \bar{q}_k + \left(\frac{\partial q}{\partial p}\right)_{h_{sat}} (p_{k+½} - p_k) \end{aligned}\right\}, \quad (25)$$

where $h_{sat} = s + Lq_{sat}$ is the saturation moist static energy. Using an extrapolation like (25) for calculating the downward transports is also more consistent with the calculation of the updrafts, where cloud air is transported upwards through level $k + ½$ with the thermal characteristics which depend only on the thermal state below that level and equally with the downdrafts which depend only on values of s and q above that level. Similarly, because of (25) the downward transport of environmental air through the same level accounts now only for thermal properties above that level. The choice of a moist adiabat for extrapolation is dictated by the property of the moist static energy which is, by convection in the absence of downdrafts, only changed through the fluxes of moist static energy as

$$\left(\frac{\partial \bar{h}}{\partial t}\right)_{cu} = -\frac{1}{\bar{\rho}} \frac{\partial}{\partial z} [M_u(h_u - \bar{h})]. \quad (26)$$

As the lines of the saturation moist static energy h_{sat} through point $(p_{k-½}, \bar{T}_{k-½})$ and the updraft moist static energy are almost parallel, apart from entrainment effects, the difference $h_u - \bar{h}$ is little affected by the vertical discretization.

The ascent in the updrafts is obtained by vertical integration of (8) over layers as indicated in Fig. 1. Starting near the surface at level with index $k_{max} - ½$ the condensation level (= lowest half-level which is saturated or supersaturated and where buyoancy is met) is determined from an adiabatic ascent. The cloud profile above cloud base is determined layer by layer by first doing a dry adiabatic ascent with entrainment and detrainment included and then adjusting temperature and moisture towards a saturated state. The cloud parcel is finally checked for positive buoyancy, that is, for excess of the virtual static energy in the cloud over the environmental value

$$(s_v)_u \geq \bar{s}_v, \quad s_v = s + C_p T(0.608\, q - l), \quad (27)$$

and cloud top is defined as the level where the parcel loses buoyancy.

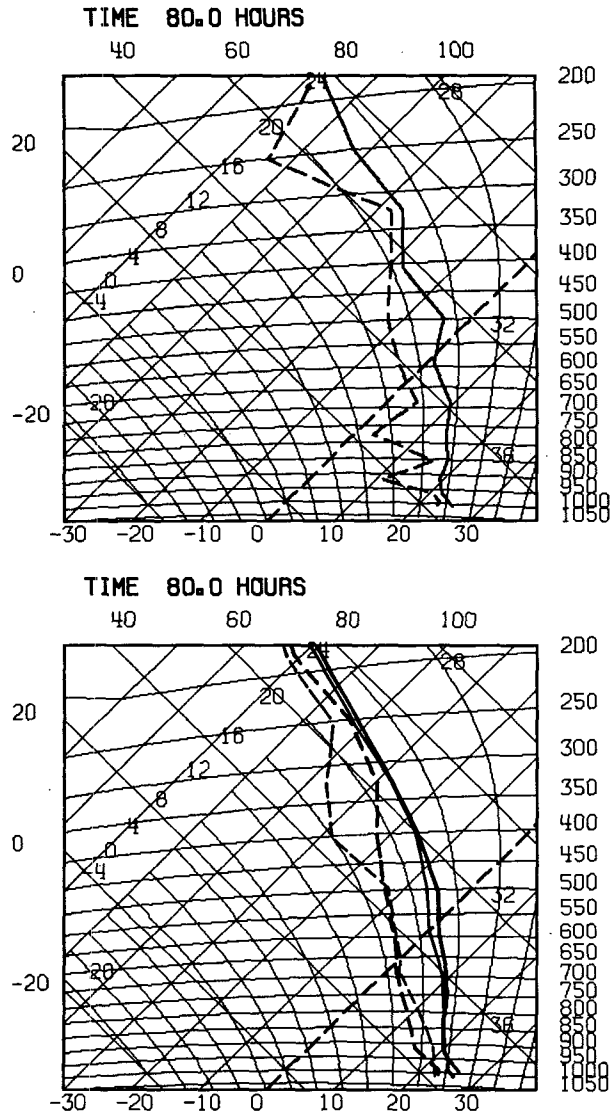

FIG. 2. GATE—simulations: Computed tephigrams at 80 h and observed tephigram at wave-ridge (thin lines) for integration with conventional centered finite difference scheme (top) and with new scheme (bottom) (see text for details).

Finally, we mention that for numerical reasons the environmental air must not be convectively unstably stratified:

$$\bar{s}_{k-½} \geq \bar{s}_{k+½}. \quad (28)$$

In fact, one of the forecasts with the ECMWF global model became numerically unstable when (28) was not imposed.

5. Numerical tests on single column datasets from field experiments

The scheme is tested on various datasets. For the purpose of verifying tropical penetrative convection we

used the two tropical datasets of composite easterly waves from the tropical eastern Atlantic (*B*-scale area of GATE, Thompson et al. 1979) and from the tropical western Pacific (Marshall Islands, Reed and Recker 1971) and for tradewind cumuli two datasets from periods of undisturbed trades during ATEX (Augstein et al. 1973; Wagner 1975) and during BOMEX (Holland and Rasmusson 1973). Extratropical organized convection is verified on a dataset for SESAME-79 (Kuo and Anthes 1984a). The purpose of these preliminary tests is to study cumulus convection in response to prescribed adiabatic forcing. This is done using a one column version of the ECMWF forecast model (i.e., a 16 level version with 3 levels in the boundary layer, the lowest being at 30 m above the surface). The basic fields of wind, temperature, specific humidity and their time changes due to various processes are interpolated to model levels and used as input for the model accordingly as well as for the purpose of verification. The prognostic method has been successfully applied by Betts and Miller (1986) and Tiedtke (1988) for developing and testing convection schemes. It should be stressed, however, that as feedbacks between convection and the large-scale flow are exluded the tests can only be considered as a first step in the validation of a cumulus parameterization. Still, using a prognostic method rather than the semiprognostic method (Lord 1982) enables us to study the response of convection to the large-scale forcing and at the same time examine how well quasi-steady thermal states are maintained. The latter may appear a trivial request but, unfortunately, is not adequately fulfilled by conventional convection schemes (Tiedtke 1988).

a. Tropical penetrative convection (GATE, West Pacific)

We use the two composite wave datasets from the eastern Atlantic (GATE) and the western Pacific (Marshall Islands). Both datasets are similar as they both contain periods where penetrative convection interacts with the large-scale flow in connection with the passage of easterly waves. The synoptical flows, particularly the large-scale ascent, are quite different, however, which causes distinct differences in the vertical profiles of convective heating as the maximum heating is displaced to higher levels over the western Pacific compared to the Atlantic (Thompson et al. 1979). Unfortunately the Pacific dataset is of poorer quality (see below) and therefore the results are less conclusive.

The numerical tests consist of time integrations with the one-column model where only cumulus convective heating and drying are calculated and all other processes, that is, temperature and moisture tendencies due to adiabatic processes, surface heat and moisture fluxes and radiation are prescribed. All integrations start from the thermal state of the wave-ridge and extend over a whole wave period (i.e., 80 h for GATE and 120 h for the Marshall Islands). The convective forcing in terms of precipitation and vertical profiles of convective heating and drying can be compared against diagnosed values. We will also compare computed convective mass fluxes with estimates from observational studies.

Figures 3–5 show convective precipitation and vertical profiles of heating and drying as a function of time. Convective precipitation (Fig. 3) is compared with two estimates derived (i) from the moisture budget and (ii) from the sensible heat budget. The two estimates differ due to data problems for calculating the various terms in the budget equations for sensible heat and moisture. The differences are rather small for the GATE data but large for the Marshall Island data as the total moisture supply by advection and surface fluxes is much too small to balance the diagnosed condensational heating and equally the observed precipi-

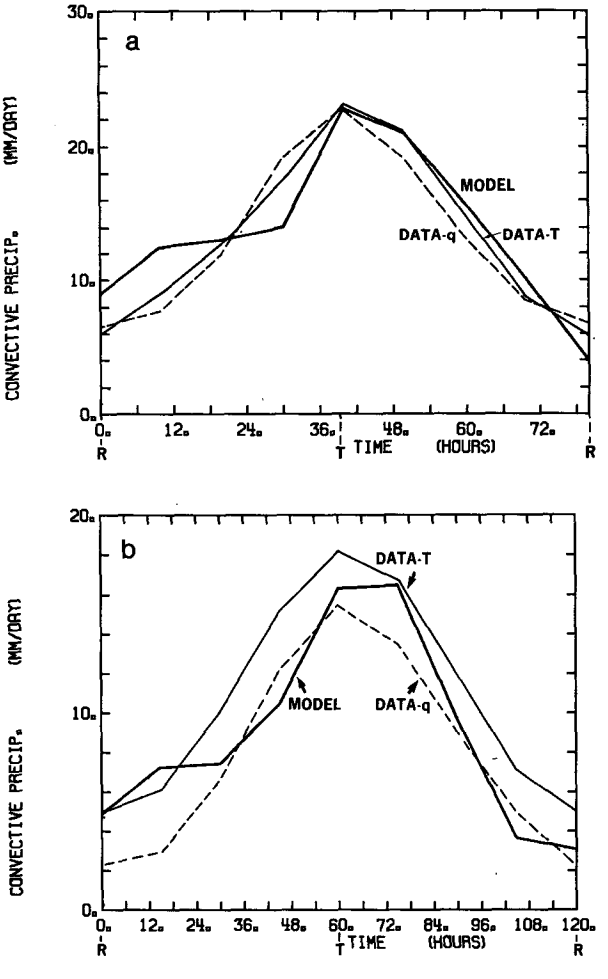

FIG. 3. (a) GATE—simulation: Time evolution of computed precipitation rate (solid line) and values diagnosed from moisture budget (dashed line) and heat budget (thin line) based on data by Thompson et al. (1979). Times of passage of ridge and trough are indicated by *R* and *T*, respectively. (b) As in (a) but for Marshall Islands data. Diagnosed values are based on data by Reed and Recker (1971).

tation (Reed and Recker 1971). The imbalance is as large as the contribution from the moisture surface fluxes itself. When we compare the computed precipitation rates against these estimates we find that the computed values for GATE (Fig. 3a) are within the accuracy of the diagnosed values except behind the ridge at the beginning of the forecast when the computed values are much larger than both estimates. The excessive precipitation indicates that penetrative convection is dominant behind the ridge, which is not confirmed by observations showing shallow convection to be more active (Johnson 1980). Penetrative convection is overestimated because in the presence of moisture convergence, even when it is weak as in the case behind the ridge, the total moisture supply from surface evaporation and large-scale convergence is assumed to go into penetrative convection. In order to account for both types of convection simultaneously the closure would have to be refined accordingly, which is an area of further development. After the initial period computed and diagnosed values are much closer and the strong convective activity in the wave trough and the decrease in intensity towards the ridge region are well reproduced. Also there is no longer excessive precipitation towards the wave ridge as noticed behind the ridge. For the western Pacific we find that the computed precipitation rates agree well with the estimates from the moisture budget but are much smaller than required to maintain the thermal state (Fig. 3b).

In order to verify the vertical profiles of convective heating and drying we compare the computed heat source and moisture sink with those diagnosed from the data. Differences between computed and observed values are only due to convection since all other processes (i.e., radiation and boundary layer turbulence) are identical. For GATE we find good agreement between simulated and observed convective heating and drying after the initial period (Figs. 4a and 4b). The maximum diabatic heating in the wave trough at 600 mb in excess of 8°K day^{-1} is well predicted, as are the weak values in the ridge region. Averaged over the whole period we find that the convective heating is larger than observed in the middle and upper tropospheres by 0.5°K day^{-1}. The moisture sink is slightly

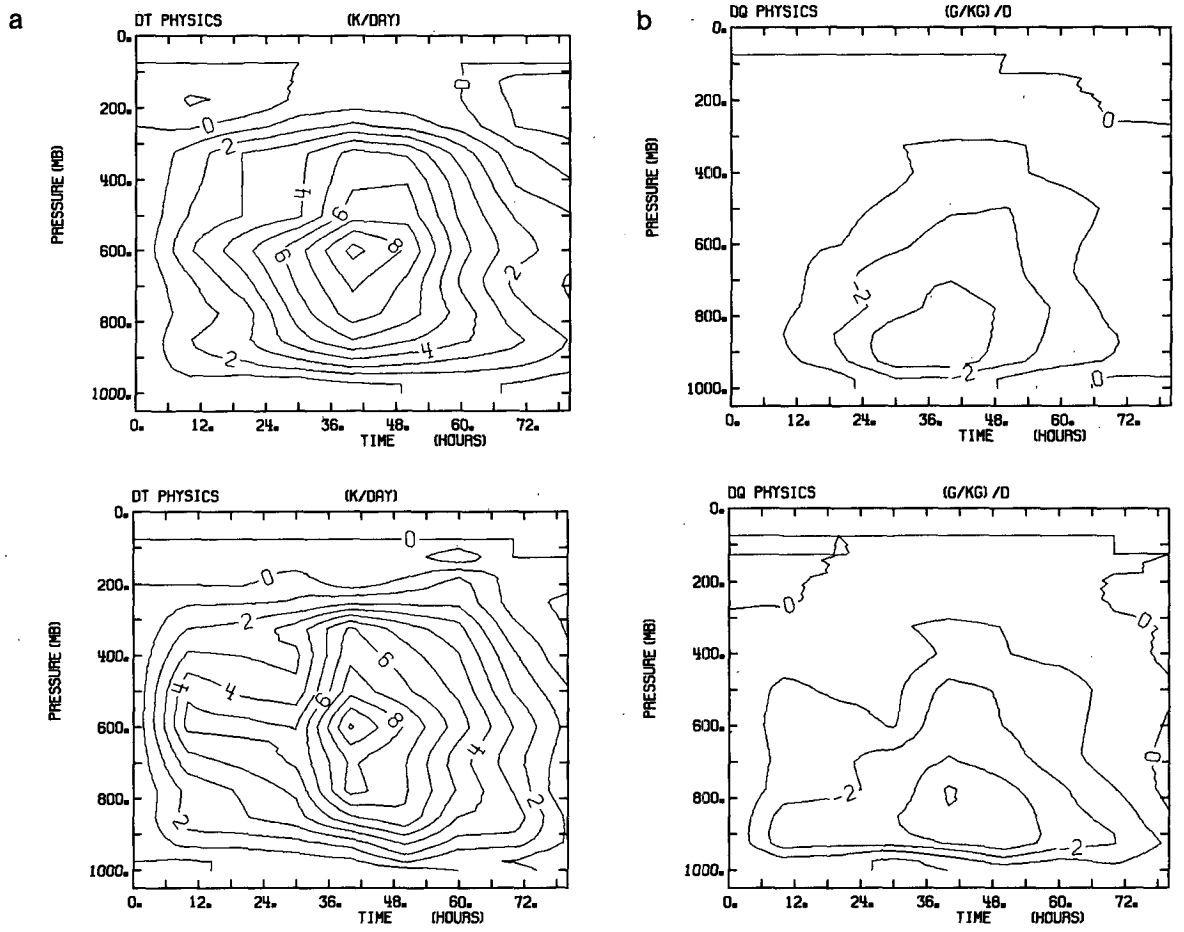

FIG. 4. (a) GATE–simulation: Time–height cross section of computed and diagnosed heat source Q_1 (K day^{-1}), diagnosed values (top) are from data by Thompson et al. (1979). (b) As in (a) but for diabatic moisture sink Q_2 (g kg^{-1} d^{-1}).

stronger at lower levels than observed and as a result the lower troposphere becomes slightly drier than observed (Fig. 2). In the upper troposphere we find the opposite tendency of excessive moistening (Fig. 2). The errors in the time averaged forcing are largely due to the excessive convective heating and drying behind the ridge.

For the western Pacific computed and diagnosed fields cannot agree simultaneously for both, moisture and heat, because of inconsistencies in the data as apparent in the precipitation estimates corresponding to the diagnosed values of net diabatic heating and net diabatic drying (Fig. 3b). Despite the obvious data deficiencies there is a good agreement of the time evolution and vertical distribution of the diabatic heating and drying (Figs. 5a and 5b). The most important result is that the maximum heating in the wave trough occurs as observed at considerably higher levels than for GATE. As shown below this upward shift coincides with a similar shift of the maximum convective mass flux to higher levels as observed.

As found in previous studies (e.g., Yanai et al. 1973; Ogura and Cho 1973) the effect of convection on the large-scale heat and moisture field is predominantly through heating and drying as a result of cumulus-induced subsidence in the environment. Therefore, if mass flux schemes are to be successful in reproducing the convective heating and drying, they must represent correctly grid-scale averages of convective mass fluxes. Cumulus mass fluxes are not observed and difficult to diagnose but some estimates are available (e.g., Cho and Ogura 1974; Johnson 1976, 1980; Chen 1985). Figure 6a shows for GATE computed and diagnosed mass fluxes. Convective updrafts are well predicted when compared to estimates by Johnson (1980), for example, the maximum in excess of 10 mb h^{-1} occurs as diagnosed in the wave trough in the midtroposphere. The mass flux at cloud base in the ridge region associated with shallow convection is much smaller than diagnosed, though. Cumulus downdrafts agree fairly well with regard to intensity, time evolution and height from which they originate. The computed updraft mass flux for the Pacific (Fig. 6b) has a similar distribution with maximum values in the wave trough and smaller values in the ridge region. The maximum in the trough occurs at higher levels, however, and consequently the

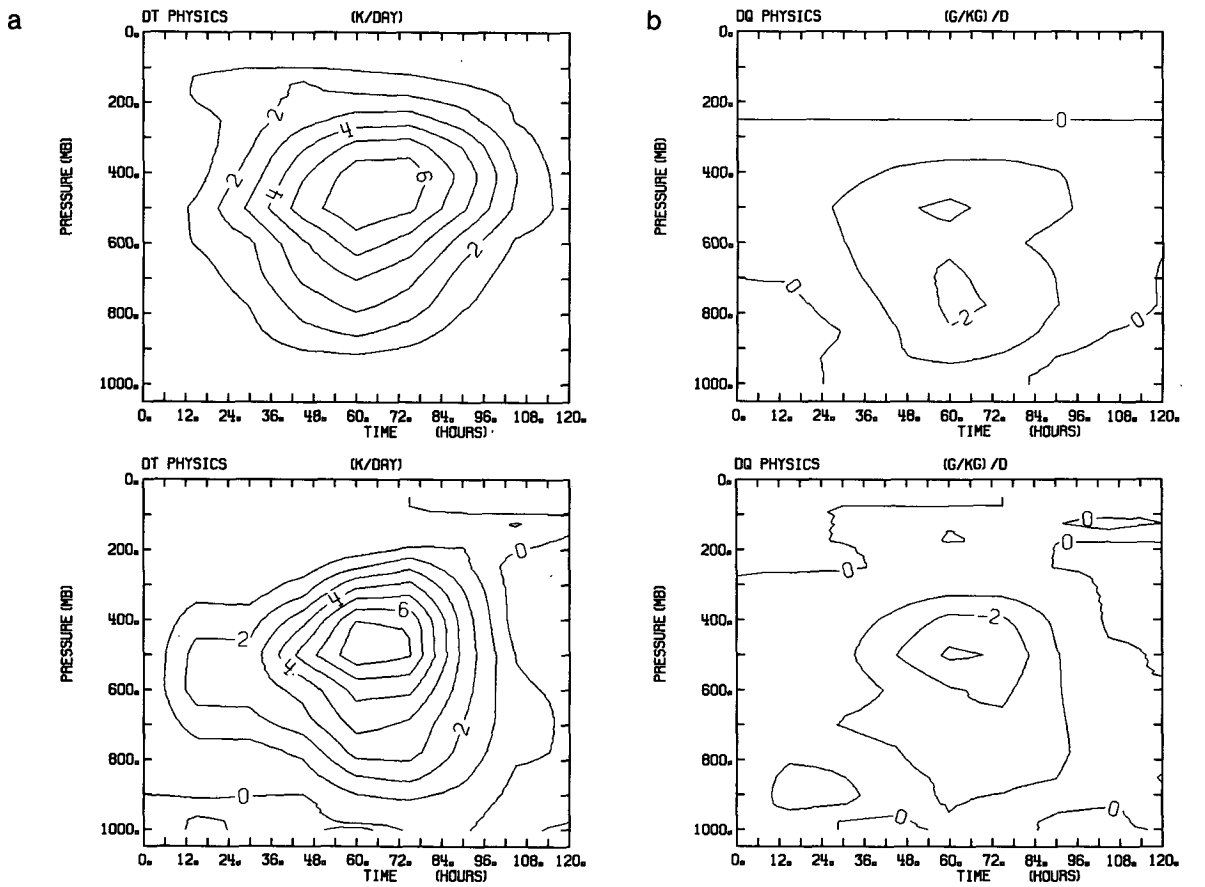

FIG. 5. (a) As in Fig. 4a, but for Marshall Islands—simulation. Diagnosed values are from Reed and Recker (1971). (b) As in (a) but for moisture sink Q_2 (g kg^{-1} d^{-1}).

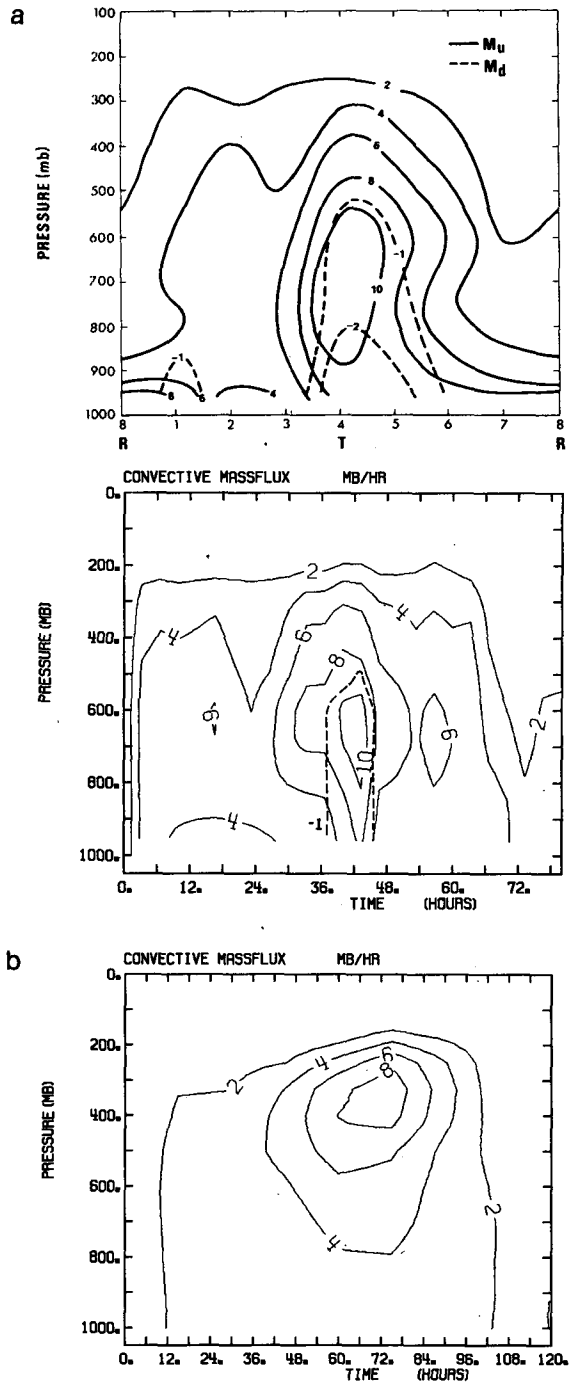

FIG. 6. (a) GATE—simulation: Time–height cross section of convective upward mass flux (solid lines) and downward mass flux (dashed lines) for model (bottom) and as diagnosed by Johnson (1980). Units are mb h^{-1}. (b) Marshall Islands—simulation: Time–height cross section of computed convective mass flux (mb h^{-1}).

net detrainment from penetrative clouds, as indicated by the decrease of mass flux with height, is concentrated in a rather thin layer above 300 mb compared to GATE where detrainment occurs over a deeper layer starting already at 600 mb. Magnitude and vertical distribution of the mass flux in the wave-trough are in good agreement with estimates from diagnostic studies given by Johnson (1976, Fig. 6).

The realistic reproduction of the different profiles of convective mass fluxes and convective heating diagnosed over the Atlantic and Pacific indicates that the closure assumptions employed are realistic. In particular the agreement of diagnosed and computed mass flux profiles seem to justify the entrainment assumption in connection with large-scale flow convergence.

As in most parameterizations, there is the question about the uncertainty introduced by disposable parameters. Here we are concerned with parameters for specifying the conversion from cloud droplets to rain drops (10), the turbulent entrainment and detrainment rates in updrafts (15) and downdrafts (18) and the intensity of the downdrafts (16). Sensitivity experiments carried out for GATE and West Pacific show that the net convective heating depends little on the assumptions about the generation of precipitation. The turbulent entrainment/detrainment rates are only disposable within a small range of values and we find that, for example, when ϵ_u and δ_u in (15) are increased by a factor of 2, the net convective heating is hardly affected in the lower and middle troposphere but penetrative convection becomes weaker. The disposable parameter γ in (16) which determines the intensity of the downdrafts, however, may cause larger uncertainties in the parameterization. Experiments performed with different values for γ ($\gamma = 0, \gamma = -0.2, \gamma = -0.4$) indicate that the downdrafts have a significant influence on the vertical profile of convective heating, as they cause less net heating in the lower and middle troposphere and more heating in the upper troposphere. The enhanced heating at higher levels occurs as a result of stronger updrafts in connection with a different boundary moisture balance in the presence of downdrafts through (19). From the differences in heating (i.e., 0.5°K day^{-1} at several levels) we conclude that the uncertainty of the downdraft parameter γ can cause errors in the net diabatic heating of the order of 10% of its value. It should be noted, however, that this estimate is obtained with a model where feedbacks with the boundary layer turbulence and the large-scale flow are ignored, whereas downdrafts are likely to be more important in a fully prognostic model.

b. Tradewind cumuli (ATEX, BOMEX)

Shallow convection is verified on the two datasets from BOMEX and ATEX. Both datasets are from undisturbed periods of Atlantic trades where the synoptic scale flow was steady throughout the period and the thermal structure of the lower troposphere was essentially maintained by a balance of the mean atmospheric downward motion and the turbulent and convective mixing from below. Convection has essentially a de-

stabilizing effect on the thermal structure of the lower troposphere by cooling the upper cloud layer and inversion layer through evaporation of clouds and turbulent heat fluxes and in this respect differs basically from tropical penetrative convection which stabilizes the atmosphere. This difference may explain that penetrative convection schemes like the Arakawa–Schubert scheme and the Kuo scheme fail to represent tradewind convection for the ATEX and BOMEX data (Tiedtke 1988). On the other hand, simple parameterizations like those based on an eddy diffusion approach (Tiedtke et al. 1988) or by relaxation to typical convective profiles (Betts 1986; Betts and Miller 1986) can realistically reproduce the overall effect of tradewind cumuli on the large-scale flow as shown for the BOMEX and ATEX data. In order to verify the new convection scheme we follow the previous studies by Betts and Miller (1986) and Tiedtke (1988). Therefore, we use the ECMWF one-column model and study convection in response to prescribed forcing due to large-scale processes and radiation. Boundary layer turbulence is parameterized as in the ECMWF operational forecast model (Louis et al. 1982), whereas convection is parameterized by the new mass flux scheme. As both datasets refer to undisturbed trades in a quasi-steady state, the tendencies of temperature and moisture tendencies due to large-scale processes and radiation are kept constant in time. The data represent 5-day means and the model is accordingly integrated for 5 days. We compare the simulated and observed vertical profiles of temperature and moisture and study in particular how well the observed steady state is reproduced and maintained by convection.

Figure 7 shows for BOMEX the thermal structure for the lower troposphere produced by the model ($\beta = 0.3$) together with the observed mean state which has also been used as the initial state in the forecasts. Also included are soundings from integrations for little penetration of convective clouds into inversion layer ($\beta = 0.1$), no penetration at all ($\beta = 0$) and an integration without the effects of shallow convection. The agreement of the predicted state ($\beta = 0.3$) with the observed state is good although the inversion is slightly weaker than observed. The model does not maintain a perfect steady state as temperature and moisture content slowly increase with time. The role of convection for heat and moisture is evident from Fig. 8. The vertical profile of convective heating shows heating in the boundary layer and in the lower part of the cloud layer and cooling above where it compensates the net heating by subsidence and radiation. Moisture supplied to the lower levels through surface evaporation is transported upward into the cloud layer and the inversion layer where it counterbalances the drying due to subsidence. By transporting moisture upward the moisture supply through surface fluxes is strongly enhanced (i.e., by more than 40%), as is evident by comparing the computed moisture flux with that obtained in the simulation where the effects of convection are neglected (Table 1). In the simulation without convection moisture is supplied only to the layer below 920 mb, which therefore becomes totally saturated (Fig. 7). The disposable parameter β, which determines the intensity of cloud penetration into the inversion layer, introduces an element of uncertainty into the parameterization scheme. In fact the simulated thermal state and the total moisture budget (Table 1) are rather sensitive to the choice of β. In the case where overshooting of con-

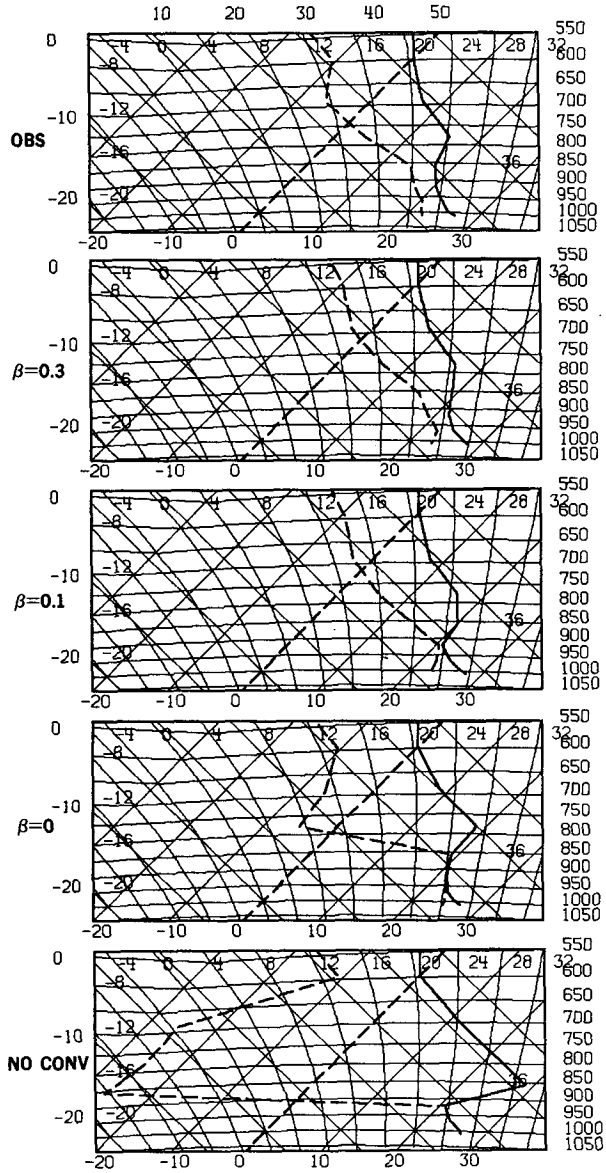

FIG. 7. BOMEX—simulation: Observed and computed tephigrams in lower troposphere for new scheme ($\beta = 0.30$) at 120 h. Observed state is mean over 5 days of undisturbed trades during BOMEX after Holland and Rasmusson (1973). Shown are also soundings for simulation with weak overshooting of convective elements above zero buoyancy level ($\beta = 0.1$), with no overshooting ($\beta = 0$) and without the effects of shallow convection (NO CONV).

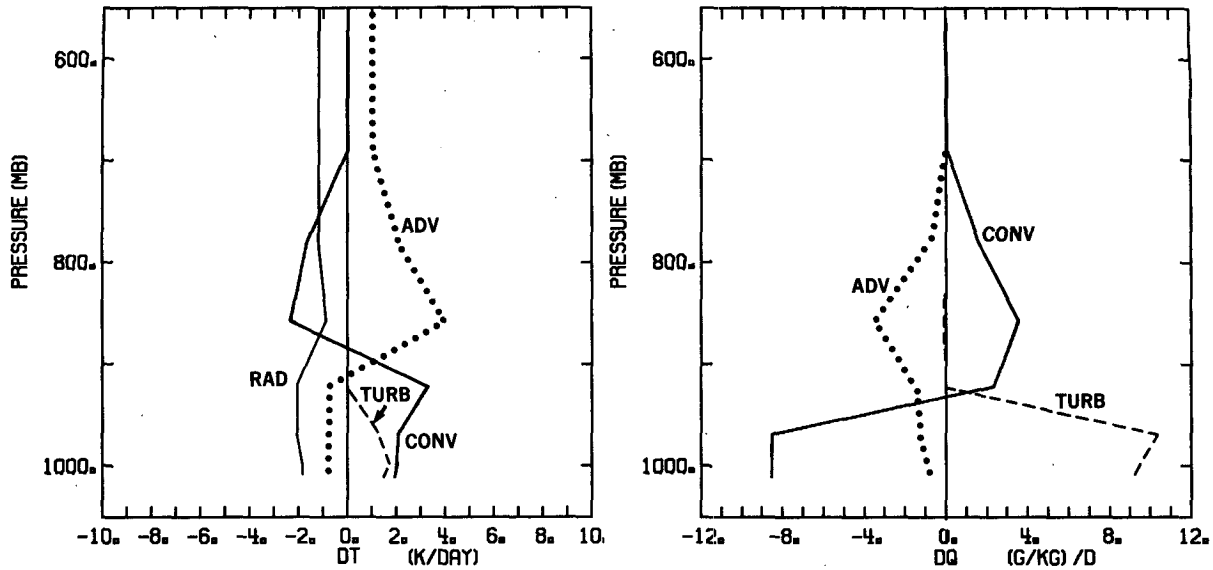

FIG. 8. BOMEX—simulation: Vertical distribution of temperature and moisture tendencies due to advection (ADV), boundary layer turbulence (TURB), radiation (RAD) and convection (CONV) averaged over the first 24 h. Contributions from advection and radiation are as diagnosed by Holland and Rasmusson (1973).

vective elements is absent ($\beta = 0$), the cloud layer becomes totally saturated and the inversion strengthens. With increasing values of β the cloud layer becomes drier and the inversion is increasingly eroded.

The synoptic conditions during ATEX are similar but exhibit significant differences in that the subsidence inversion is stronger in connection with stronger heating and drying by the mean subsidence (Figs. 9 and 10). As a result, convection is more suppressed than during BOMEX. The model is only partly successful in reproducing the observed mean thermal state under these more suppressed conditions. Boundary layer and lower part of the cloud layer agree well with observation, but the air below and above the inversion becomes slowly but gradually warmer and drier (at 850 mb by 0.40°K day^{-1} and 0.15 g kg^{-1} day^{-1}, respectively) and the inversion intensifies (Fig. 9). The reason for the imbalance is not known. If we rule out errors in the forcing (radiative cooling, adiabatic heating and drying) and in the parameterization of boundary layer processes the error must be in the parameterization of convection as it is too weak to counteract the other processes. Areas which might be responsible for the deficiency are the simplicity of the cloud model, the assumptions about cloud base mass flux and the penetration of clouds into the inversion layer or the omission of processes such as the vertical advection and reevaporation of cloud water. It is significant that the moisture supply through the turbulent surface fluxes to which convection is closely linked is also too weak (Table 2). Despite the imbalance the predicted thermal state at day 5 shows the typical 4-layer structure, i.e., a nearly well mixed subcloud layer, a cumulus cloud layer, an inversion and the very dry free atmosphere above (Riehl et al. 1951). This structure is only maintained when the effects of cumulus convection and overshooting elements ($\beta \neq 0$) are considered (Fig. 9). The sensitivity of the simulated thermal state to changes in the proportion of cumulus elements penetrating through the zero buoyancy level is very similar to what has been found for BOMEX, the best agreement with observations is obtained for $\beta = 0.3$ as for BOMEX (Fig. 9).

TABLE 1. BOMEX simulations: Diagnosed and computed 5-day mean surface fluxes of sensible heat and latent heat (W m^{-2}) for simulations with (i) $\beta = 0.3$, (ii) $\beta = 0.1$, (iii) $\beta = 0$ and for a simulation without convection (NO CONV). Diagnosed fluxes are those calculated from the temperature and moisture tendencies due to advection and radiation, assuming steady state conditions.

		Model			
	Diagnosed	$\beta = 0.3$	$\beta = 0.1$	$\beta = 0$	NO CONV
Sensible heat	1.6	6.0	6.1	14.3	17.3
Latent heat	153.8	171.9	171.1	157.0	98.7

c. *Extratropical organized convection (SESAME-79)*

Extratropical convection is verified on a case of intense convection in connection with severe storms over the central United States during SESAME-79, 10–11 April 1979. Again one-column integrations were performed where the temperature and moisture tendencies due to advective processes are prescribed and only convective processes are calculated. Radiative cooling

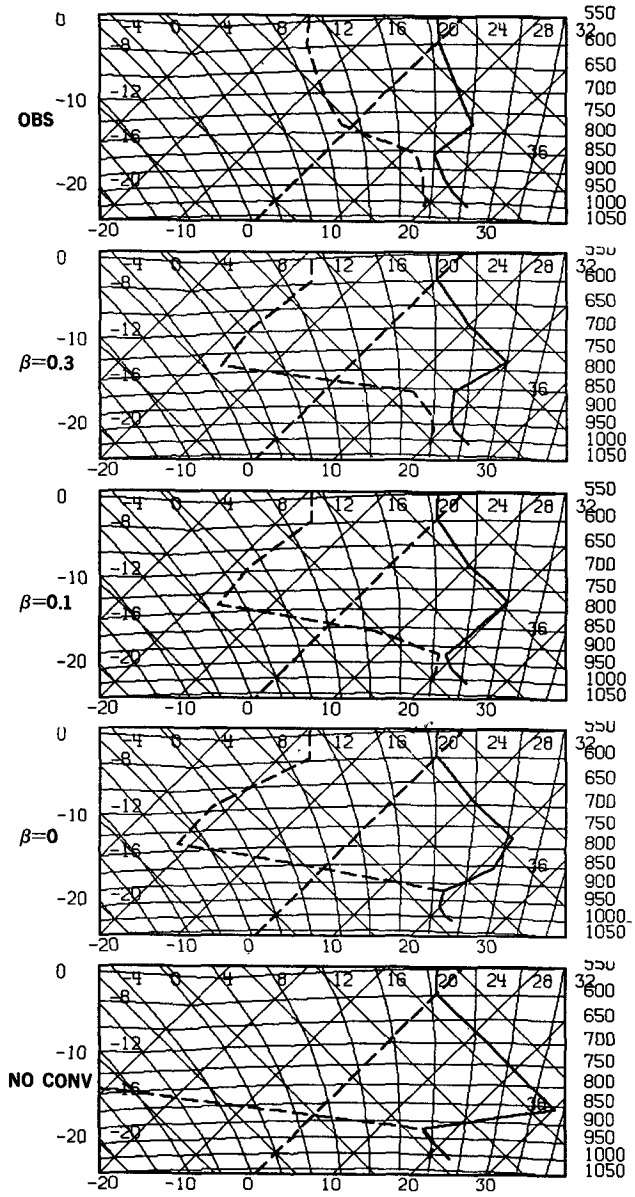

FIG. 9. ATEX—simulation: As in Fig. 7, but for ATEX. Observed sounding after Wagner (1975).

and surface fluxes are neglected. Temperature and moisture tendencies due to advection are specified using the Eulerian budget values for Box B for the period 1200 UTC 10 April to 1200 UTC 11 April, given by Kuo and Anthes (1984a). Unfortunately, the estimates of the heat and moisture budgets contain large errors (Kuo and Anthes 1984b) which impair on the verification of our computations. Precipitation was observed to be almost entirely of convective nature. As a low-level inversion persisted throughout the period, convection was presumably initiated by large-scale lifting giving a condensation level well above the boundary layer at 750 mb (Kuo and Anthes 1984a). Because of the inversion only the midlevel convection type was activated in the model with a cloud base at 770 mb.

The results of the integration, summarized in Figs. 11–13, show that the convective forcing is reproduced well within the accuracy of the diagnosed values. Computed precipitation rates are half in between the estimates from the moisture budget and the heat budget (Fig. 11), which differ largely due to data problems in particular for the heat budget calculations. As the precipitation estimates from the moisture budget are closer to the observed values (Kuo and Anthes 1984a) convection is presumably underestimated by the model. Despite the differences in the total convective heating and drying as evident in the precipitation rates, there is good agreement with regard to the time evolution and vertical distribution of convective heating and drying. The maximum of convective heating (Fig. 12a) occurs as observed at 0300 UTC 11 April (t = 15 h) near the 400 mb level although it exceeds the diagnosed value by 5°K day^{-1}. Below 400 mb convective heating decreases as diagnosed but is stronger and extends further down, although in view of the data deficiencies it is not possible to say which is more realistic. The strong net cooling diagnosed at 200 mb, of unclear origin, (Kuo and Anthes 1984a), is partly reproduced in the model as a result of convective elements overshooting the zero buoyancy level. Computed and diagnosed profiles of convective heating agree still better when averaged over the whole period (Fig. 13), although the model produces more heating in the middle troposphere. The moisture sink due to convection is also realistic in time and space (Fig. 12b) but seems to be underestimated below 800 mb, which is also apparent in its time average (Fig. 13).

An important aspect of convection for the evolution of the mesoscale and large-scale flow is the vertical separation of the diabatic moisture sink occurring at lower levels and the diabatic heat source, which occurs at much higher levels. Separation is, for this case, well reproduced by the new scheme (Fig. 13). It is worth noting that heat source and moisture sinks are vertically unseparated in an integration where convection is not parameterized, and condensational heating is only considered when the whole area becomes saturated (Fig. 13). The failure to do so is significant for mesoscale modeling where sometimes the same assumption is made, that is, convection is assumed to occur only at resolved scales as so-called "explicit condensation."

6. Global forecast experiments

Global integrations are performed with the spectral model used for operational forecasts at ECMWF. They consist of a series of 10-day forecasts at resolution T106 (i.e., 21 initial dates during 1986–1988), extended integrations (30 days) at resolution T63 for two summer and two winter dates plus a four-dimensional data assimilation run to study the influence of convection pa-

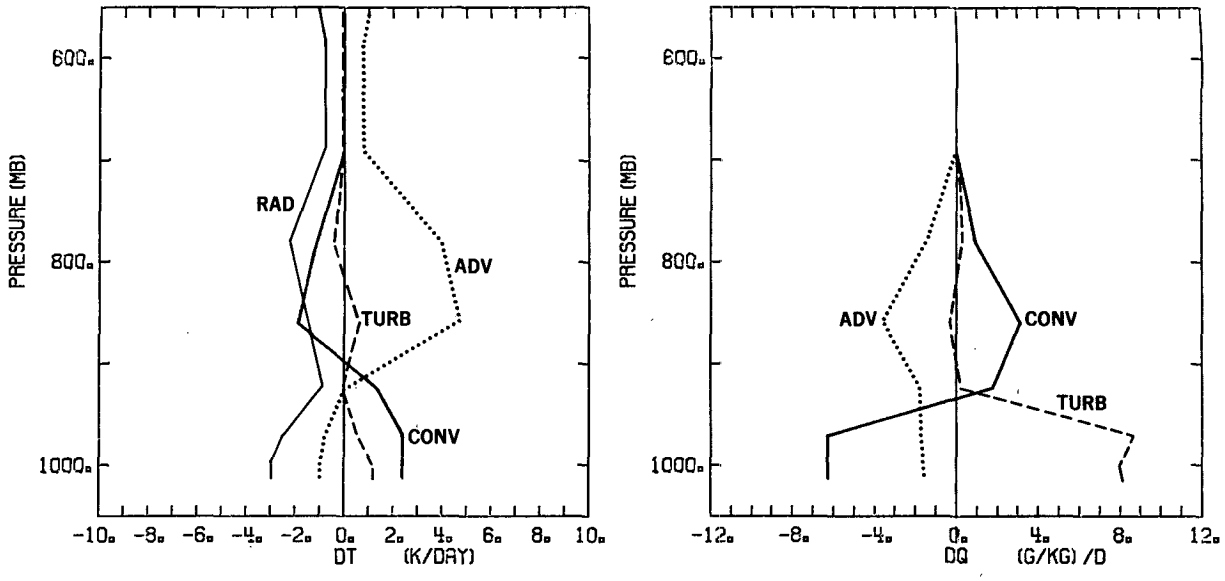

FIG. 10. ATEX—simulation: As in Fig. 8 but for ATEX. Contributions from advection and radiation are as diagnosed by Wagner (1975).

rameterization on the analysis and the spinup in the early stages of the forecast. We use the new mass flux scheme as described above but also include transports of momentum by cumulus updrafts, cumulus downdrafts and cumulus induced subsidence in the environment in exactly the same way as for moisture and dry static energy (Schneider and Lindzen 1976; Esbensen et al. 1987). This parameterization is very crude as it assumes zero pressure drag on the clouds for calculating the vertical profiles of u and v within the clouds, which may influence the cloud momentum profile above 500 mb (Shapiro and Stevens 1980). It represents, however, the dominant effects from cumulus convection. By effectively producing downgradient momentum fluxes in the tropics by penetrative convection, it acts to decelerate the large-scale zonal wind in the upper troposphere which is confirmed by diagnostic studies (e.g., Sui and Yanai 1986). Further support for the parameterization is provided by a comprehensive data study for tropical cloud clusters (Lee 1984).

TABLE 2. ATEX simulations: Diagnosed and computed 5 day mean surface fluxes of sensible heat and latent heat (W m^{-2}) for simulations with (i) $\beta = 0.3$, (ii) $\beta = 0.1$, (iii) $\beta = 0$ and for a simulation without convection (NO CONV). Diagnosed fluxes are those calculated from the temperature and moisture tendencies due to advection and radiation, assuming steady state conditions.

		Model			
	Diagnosed	$\beta = 0.3$	$\beta = 0.1$	$\beta = 0$	NO CONV
Sensible heat	13.1	2.9	6.3	9.3	19.6
Latent heat	170.1	153.6	145.4	135.4	99.8

As it is outside the scope of this paper to discuss the effect of cumulus parameterization on NWP, we shall only summarize the main results which emerged from the comparison with a conventional scheme used routinely for NWP, that is, the ECMWF operational parameterization of penetrative convection by a Kuo scheme and of shallow convection by vertical diffusion (Tiedtke et al. 1988). The new scheme is in its physical concept more realistic through the introduction of cumulus downdrafts, cumulus momentum transport and the parameterization of midlevel convection, all of which are not considered in the operational scheme. Diabatic heating by convection is assessed in terms of

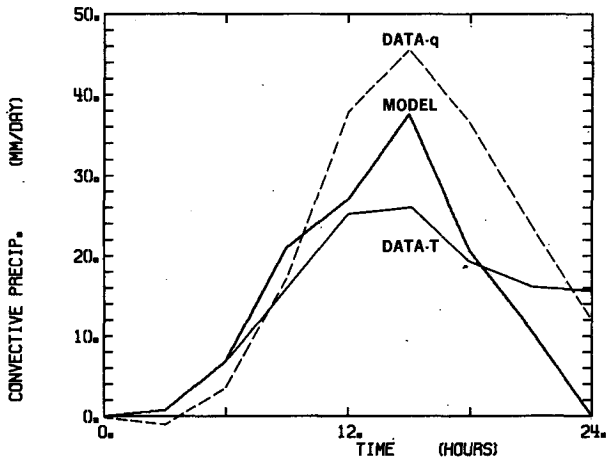

FIG. 11. SESAME-79—simulation: Time evolution of computed precipitation rate (solid line) and values diagnosed from moisture budget (dashed line) and heat budget (thin line) based on data by Kuo and Anthes (1984a).

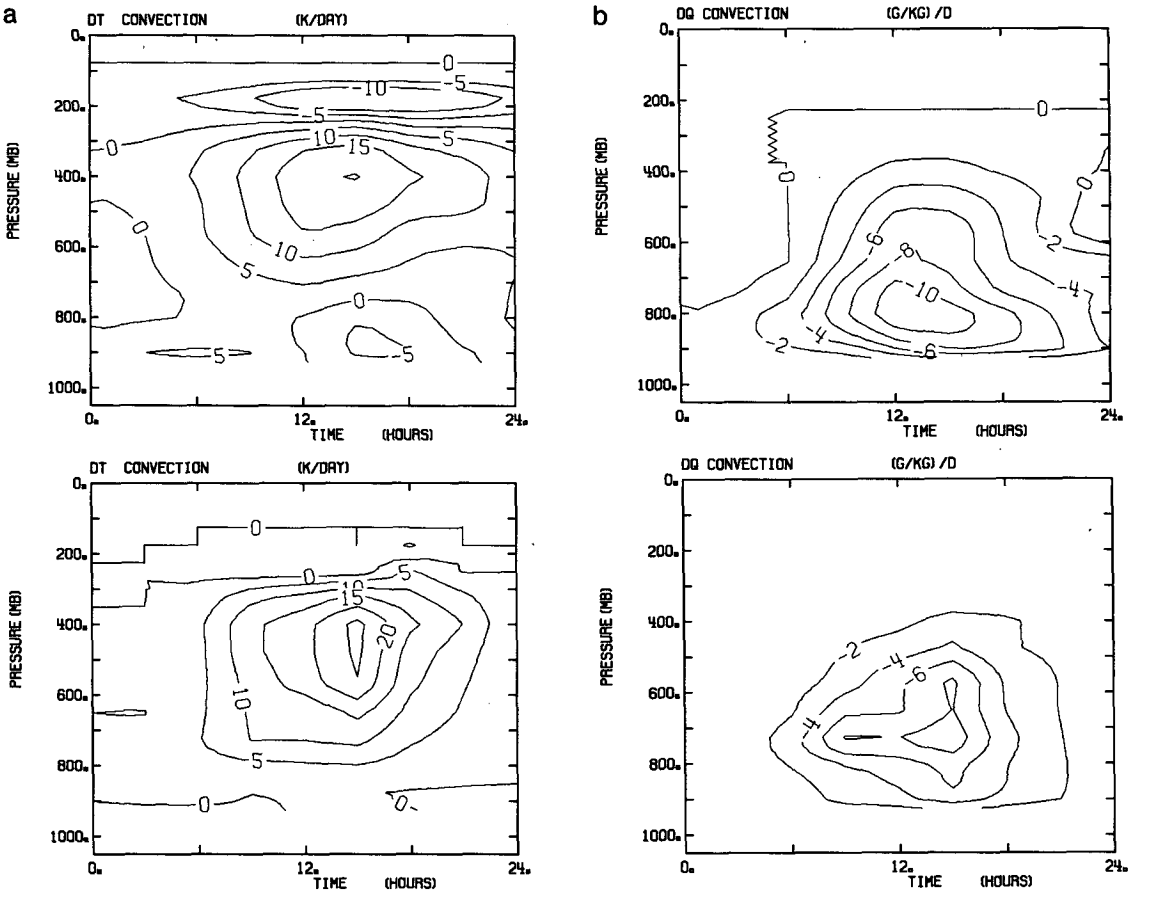

FIG. 12. (a) SESAME-79 simulation: Time–height cross section of computed and diagnosed heat source Q_1 (K d^{-1}). Diagnosed values are from Kuo and Anthes (1984a). (b) As in Panel (a), but for moisture sink Q_2 (g kg^{-1} d^{-1}).

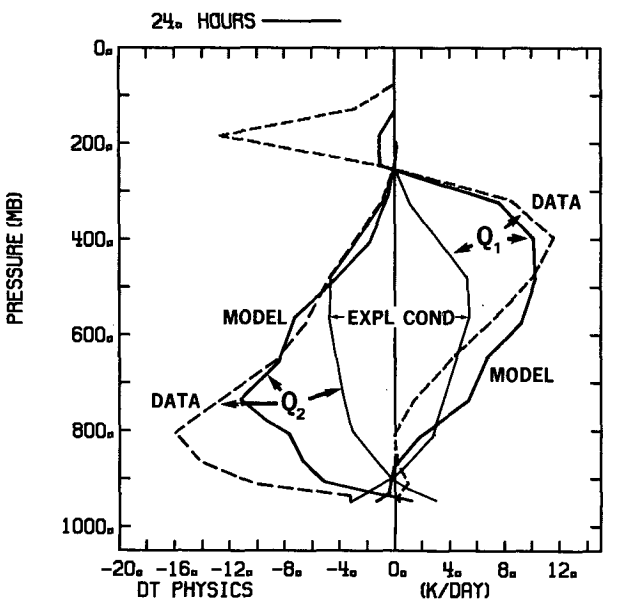

FIG. 13. SESAME—simulations: Vertical profiles of 24 h time averaged diabatic heating Q_1 and diabatic moistening Q_2 for integration with mass flux scheme (solid lines); for integration with "explicit condensation" (thin lines) and diagnosed from data by Kuo and Anthes (1984a).

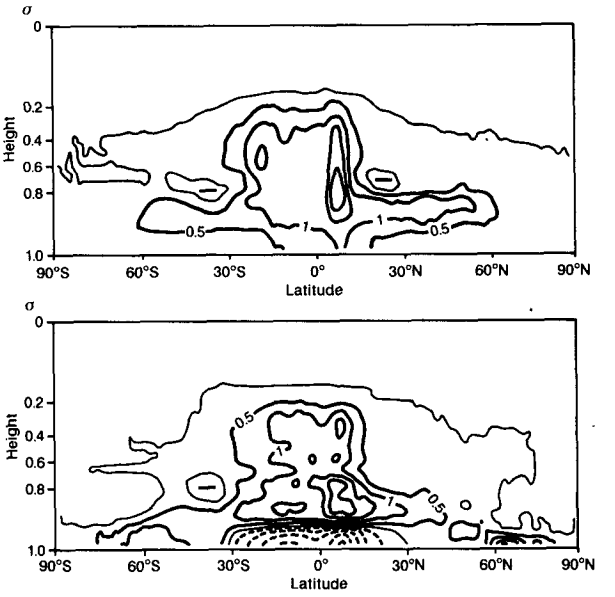

FIG. 14. Thirty-day mean convective heating (K day^{-1}) zonally averaged over all model grid points for 30 day integrations from 1200 UTC 17 January 1988. Vertical coordinate is normalized pressure. Plotting interval is 0.5°K day^{-1}, dashed lines for convective cooling. Top: mass flux scheme; Bottom: ECMWF operational convection scheme.

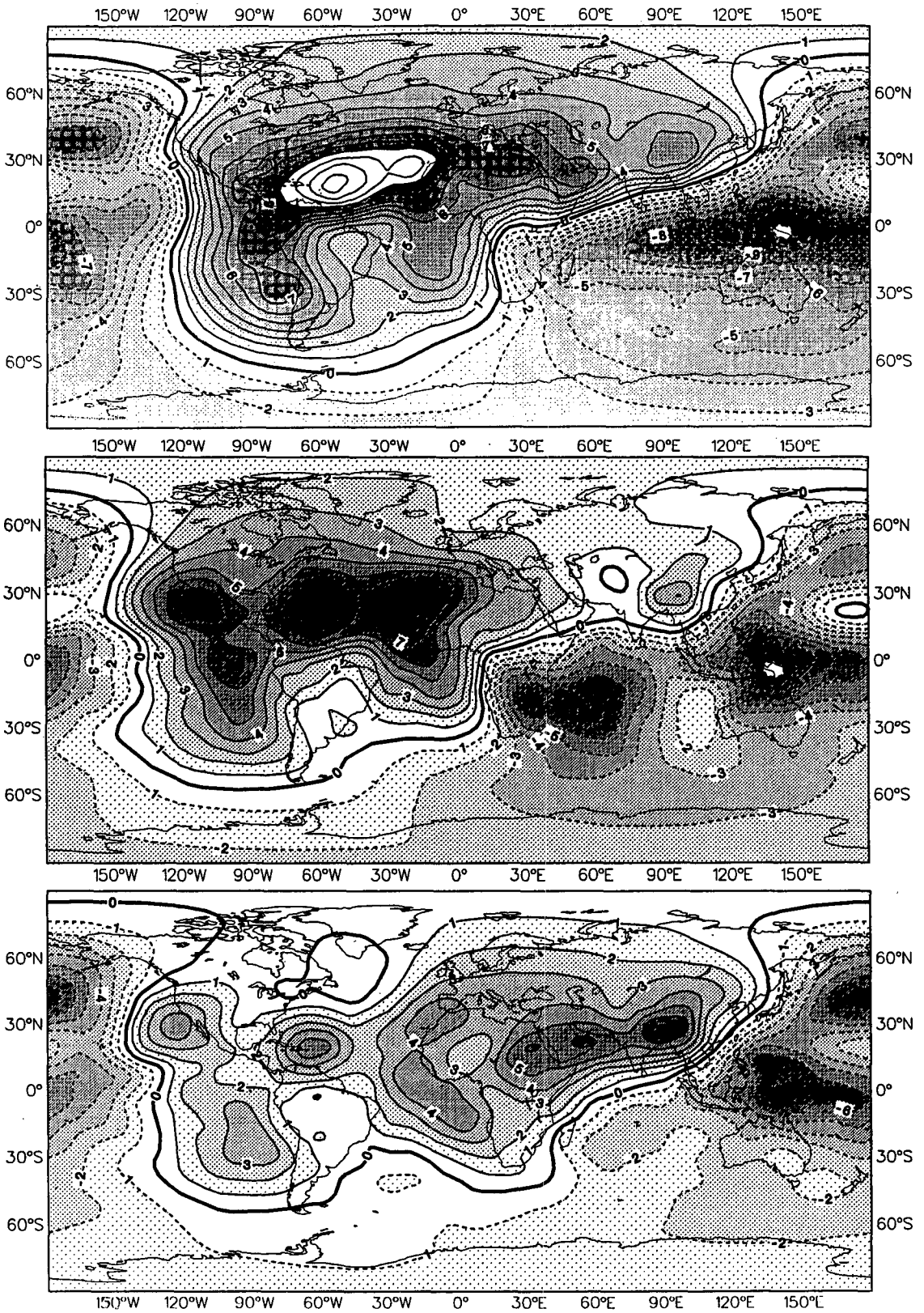

FIG. 15. Thirty-day mean velocity potential (10^6 m^2 s^{-1}) at 200 mb for the integrations with the ECMWF operational convection scheme (bottom), the mass flux scheme (middle) plus analyzed field (top).

zonal means of the time averaged heating (Fig. 14). Both schemes produce strong heating by convection in the ascending branch of the Hadley cell and a second maximum in the midlatitude belts of baroclinic disturbances. Cooling by convection occurs in the subtropics at the trade inversion in connection with shallow convection and in the subcloud layer with the Kuo scheme due to evaporation of rain. The mass flux scheme does not produce a net cooling below cloud base as the evaporative cooling is compensated by heating due to a net downward convective heat flux at cloud base which is not represented in the Kuo scheme. The convective heating in midlatitudes is stronger with the new scheme as a result of midlevel convection which again is not included in the operational scheme. In the tropics the new scheme provides more heating. The increase occurs in the convectively active areas over the West Pacific and Indian oceans and reflects a different balance between adiabatic cooling and convective heating in the ascending branches of the Hadley cell in these areas. In fact, the ascent is stronger and extends to higher levels as is clearly evident in the divergent flow at 200 mb (Fig. 15), which shows an increased upper level outflow from these areas. The circulation predicted with the new scheme agrees better with the analyzed circulation, in particular as it does

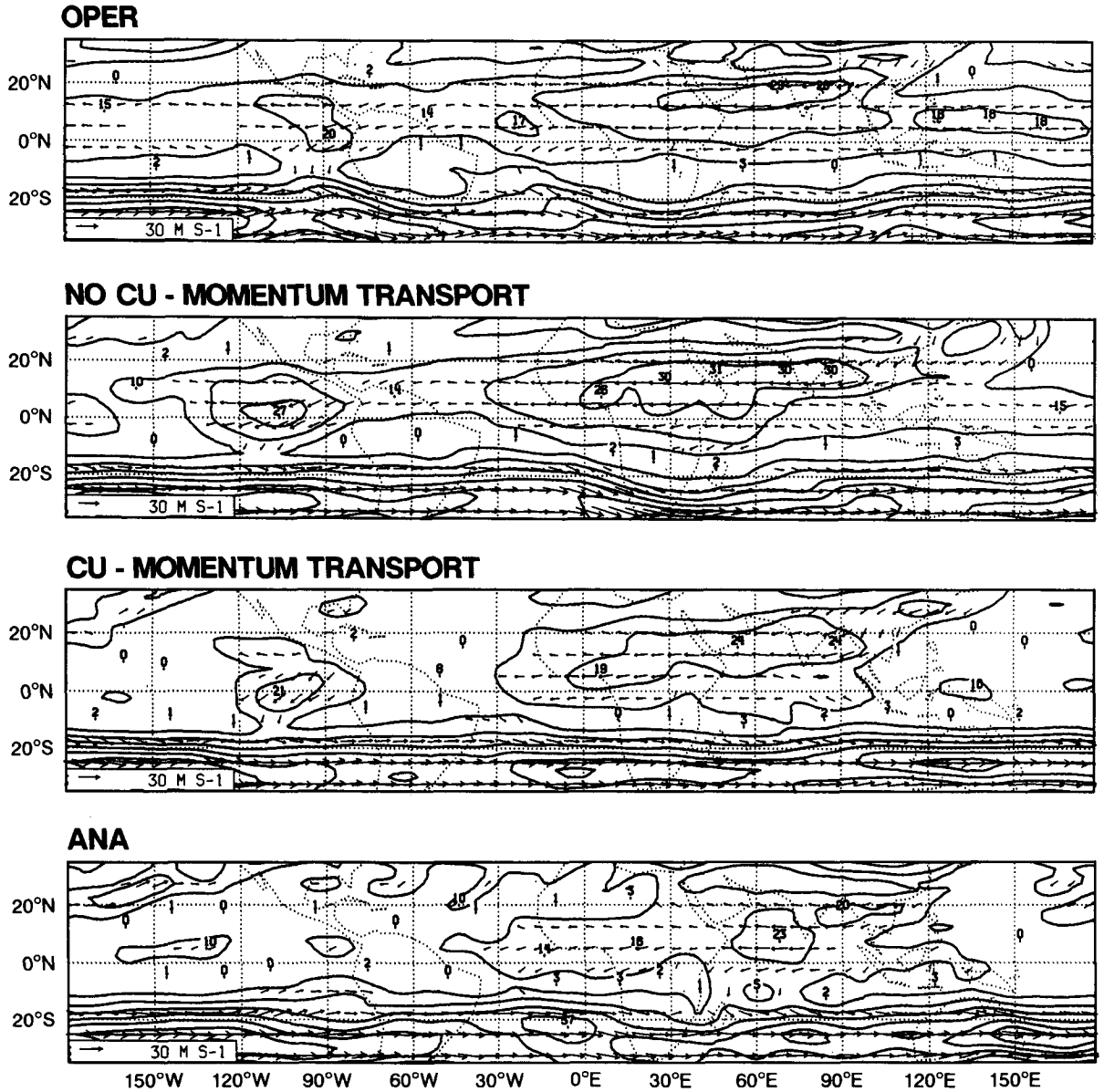

FIG. 16. The 16–30 day mean tropical flow at 200 mb for T63 integration from 1200 UTC 19 July 1987 with ECMWF operational model, mass flux scheme without cumulus momentum transport and with cumulus momentum transport plus analyzed mean flow for same period.

not collapse as with the Kuo scheme. The collapse of the circulation is a systematic feature of ECMWF operational forecasts (Arpe 1988).

The time-averaged rotational flow seems to be rather insensitive to the parameterization of convective heating, as both schemes produce, in the absence of cumulus momentum transport, wind fields that have equally large errors in the upper tropospheric zonal wind. The rotational flow, however, appears to be strongly affected by momentum forcing by cumulus convection. This has been established through sensitivity experiments for the two summer cases, where the mass flux scheme was run (i) with and (ii) without momentum transport. When momentum transport is included, the wind errors are much reduced over the Western Atlantic, South America and Pacific (Fig. 16). Similar results are obtained for the winter case but, as the wind errors are larger, the relative improvement remains smaller. It is worth noting that cumulus momentum transport had little effect on the divergent flow, neither in terms of the zonal averaged Hadley circulation nor on the intensity of their regional branches, which seems to support the findings by Thompson and Hartmann (1979).

The data assimilation experiment shows that the new parameterization influences the analysis of both mass and wind field. It produces a warmer tropical troposphere (by 0.5°K in the zonal mean) and differences in the zonal mean wind of the order of 0.5 m s^{-1}. More importantly, it has a strong effect on the internal balance of the initial flow. The balance is poor in ECMWF analyses and therefore is restored in forecasts by means

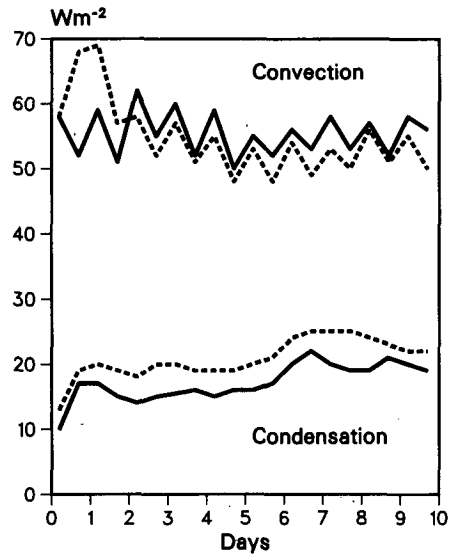

FIG. 17. Time evolution of global diabatic heating rates due to cumulus convection and large-scale condensation in forecasts with mass flux scheme after 3 days of data assimilation with mass flux scheme (full line) and with ECMWF operational convection scheme in data assimilation and forecast (dashed line), (initial date: 1200 UTC 13 February 1987).

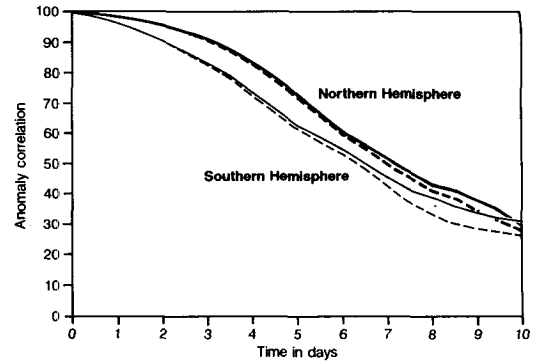

FIG. 18. Anomaly correlations of 1000–200 mb height field in the extratropical Northern and Southern hemispheres for ensemble of 21 T106 forecasts with new mass flux scheme (full lines) and with ECMWF operational convection scheme (dashed lines).

of a strong adjustment (spinup/spindown of convective heating) during the first few forecast days (Tiedtke et al. 1988). With the new scheme the balance appears to be much better as there is no indication of a spinup in the forecast starting from initial conditions based on the data assimilation with the new scheme (Fig. 17). The absence of a spinup indicates that the new scheme is fairly compatible with the assimilated observational data.

Evaluation of the pairs of T106 forecasts for the 21 initial dates shows a large spread in quality of the extratropical forecasts. In a number of cases the forecast quality decreases with the new scheme but, in the mean, an improvement for both hemispheres is evident from the ensemble of objective scores (Fig. 18). Improvements are small at day 3 but increase with forecast time. As diabatic forcing from convection can influence extratropical synoptic systems directly through deep convection at fronts and midlevel convection and indirectly in response to tropical convection, it is not clear which process contributes most. Sensitivity experiments performed for a few cases indicate that the introduction of midlevel convection is partly responsible.

7. Conclusions

Several cumulus parameterizations proposed for large-scale models in recent years are based on the mass flux approach. Although this approach because of its realistic physical concept is most attractive, its application is impeded by difficulties such as:

(i) the definition of a cumulus cloud model,
(ii) the closure assumption to derive the cloud mass flux,
(iii) the discretization of the vertical advection terms associated with cumulus induced circulations, and
(iv) the representation of the various types of convection which occur on the globe.

We have addressed some of these questions through verification of such a scheme on real data. Our results indicate that for parameterization purposes it is sufficient to describe the cloud ensemble as a bulk by a one-dimensional model. Thus, in order to obtain realistic large-scale heating fields by convection, detailed knowledge about the cumulus ensemble seems not to be a necessary requisite, which makes the parameterization task much easier since the components of the cumulus ensemble must then not be explicitly described as is for instance done in the Arakawa–Schubert scheme. Furthermore, our results suggest that a crude representation of the bulk cloud properties can already provide realistic convective forcing. For example, in case of penetrative convection we imposed a unimodal distribution of only deep clouds and we found little indication that the lack of shallow clouds causes excessive drying in the lower troposphere as noted with the Arakawa–Schubert scheme (Lord 1982).

The specification of the closure is an important and still unsolved problem. Although this paper cannot provide the answer as to what is the best closure, the results indicate that a moisture budget hypothesis can provide a realistic framework for determining the cloud mass flux. We found it necessary, however, to differentiate between the various types of convection. The assumptions were that penetrative clouds are maintained by organized entrainment through cloud base and cloud edges in connection with large-scale convergent flow, that shallow cumuli are entirely rooted in the boundary layer and are maintained by moisture supply through surface evaporation and that midlevel convection is initiated by dynamical lifting of moist air to the level of free convection and is maintained by large-scale moisture convergence through entrainment similar to tropical penetrative convection. The assumptions about penetrative and shallow convection as well as extratropical convection seem to be well justified by our numerical experiments.

Discretization of the vertical advection terms poses a particular problem for mass flux schemes. Our results show that the vertical profiles of convective heating and drying are highly sensitive to the choice of a finite difference scheme for the subsidence terms which, if not carefully made, can largely impair the quality of the parameterization scheme.

Verification of cumulus parameterization schemes depend largely on the availability of observational datasets. Unfortunately adequate data are sparse and not always of sufficient quality. The quality of the Marshall Islands dataset, which is frequently being used for convection studies, is poorer than is acceptable for a detailed study and therefore the data were only of limited use. Similar restrictions must be made for the SESAME-79 data. The need for further datasets became very much apparent during this study.

Although the main purpose of this study has been to address some basic questions related to cumulus parameterization, the scheme presented here has been developed with the further purpose to provide a practical scheme for global forecast models. Comparisons with a conventional convection scheme used for NWP at ECMWF show that the diabatic forcing of the tropical large-scale flow appears more realistic with the new scheme. In particular the vertical circulation in response to heat sources over the West Pacific and Indian oceans is more realistic, being stronger and extending to greater heights as already indicated in the one-column experiments with the Pacific data. The test within the ECMWF data assimilation suite indicates that the scheme is fairly compatible with observational data producing well-balanced initial conditions with the result that the spinup in the early stages of the forecast is much reduced compared to the ECMWF operational convection scheme. The introduction of cumulus momentum transport appears to have a strong effect on the maintenance of the rotational flow in the tropics and suggests the need for further studies.

Acknowledgments. The author is grateful to Dr. Lennart Bengtsson, Dr. Martin Miller, J.-F. Geleyn and two anonymous referees for their valuable comments on the manuscript.

REFERENCES

Arakawa, A., and W. H. Schubert, 1974: Interaction of a cumulus cloud ensemble with the large-scale environment: Part I. *J. Atmos. Sci.*, **31**, 674–701.

——, and J. M. Chen, 1987: Closure assumptions in the cumulus parameterization problem. *Short- and Medium-Range Numerical Weather Prediction,* WMO/IUGG NWP Symp., Tokyo, Suppl. to *J. Meteor. Soc. Japan,* 107–131.

Arpe, K., 1988: Planetary-scale diabatic forcing errors in the ECMWF model. *ECMWF Workshop on Diabatic Forcing,* Reading, U.K., 103–150. [Available from ECMWF, Shinfield Park, Reading, Berkshire, U.K.]

Augstein, E., H. Riehl, F. Ostapoff and V. Wagner, 1973: Mass and energy transports in an undisturbed Atlantic trade-wind flow. *Mon. Wea. Rev.*, **101**, 101–111.

Bennets, D. A., and B. J. Hoskins, 1979: Conditional symmetric instability—a possible explanation for frontal rainbands. *Quart. J. Roy. Meteor. Soc.*, **105**, 945–962.

——, and J. C. Sharp, 1982: The relevance of conditional symmetric instability to the prediction of meso-scale frontal rainbands. *Quart. J. Roy. Meteor. Soc.*, **108**, 595–602.

Betts, A. K., 1986: A new convective adjustment scheme. Part I: Observational and theoretical basis. *Quart. J. Roy. Meteor. Soc.*, **112**, 677–691.

——, and M. Miller, 1986: A new convective adjustment scheme. Part II: Single column tests using GATE Wave, BOMEX, ATEX and arctic air-mass data sets. *Quart. J. Roy. Meteor. Soc.*, **112**, 693–709.

Browning, K. A., M. E. Hardman, T. W. Harrold and C. W. Pardoc, 1973: The structure of rainbands within a mid-latitude depression. *Quart. J. Roy. Meteor. Soc.*, **99**, 215–231.

Chen, Y.-L., 1985: Diagnosis of the net cloud mass flux in GATE. *J. Atmos. Sci.*, **42**, 1757–1769.

Cheng, L., T.-C. Yip and H.-R. Cho, 1980: Determination of mean cumulus cloud vorticity from GATE A/B-scale potential vorticity budget. *J. Atmos. Sci.*, **37**, 797–811.

Cho, H.-R., and Y. Ogura, 1974: A relationship between cloud activity and the low-level convergence as observed in Reed–Reckers' composite easterly waves. *J. Atmos. Sci.*, **31**, 2058–2065.

Emanuel, K. A., 1982: Inertial instability and mesoscale convective systems. Part II: Symmetric CISK in a baroclinic flow. *J. Atmos. Sci.*, **39**, 1080–1097.

Esbensen, S. K., L. J. Shapiro and E. I. Tollrud, 1987: The consistent parameterization of the effects of cumulus clouds on the large-scale momentum and vorticity fields. *Mon. Wea. Rev.*, **115**, 664–669.

Foster, D. S., 1958: Thunderstorm gusts compared with computed downdraft speeds. *Mon. Wea. Rev.*, **86**, 91–94.

Fritsch, J. M., and C. G. Chappell, 1980: Numerical prediction of convectively driven mesoscale pressure systems. Part I: Convective parameterization. *J. Atmos. Sci.*, **37**, 1722–1733.

Geleyn, J.-F., C. Girard and J.-F. Louis, 1982: A simple parameterization of moist convection for large-scale atmospheric models. *Beitr. Phys. Atmos.*, **55**, 325–334.

Herzegh, P. H., and P. V. Hobbs, 1980: The mesoscale and microscale structure and organization of clouds and precipitation in mid-latitude cyclones. Part II: Warm-frontal clouds. *J. Atmos. Sci.*, **37**, 597–611.

Holland, J. Z., and E. M. Rasmusson, 1973: Measurements of the atmospheric mass, energy and momentum budgets over a 500 km square of tropical ocean. *Mon. Wea. Rev.*, **101**, 44–55.

Houze, R. A., Jr., and A. K. Betts, 1981: Convection in GATE. *Rev. Geophys. Space Phys.*, **19**(4), 541–576.

——, and P. V. Hobbs, 1982: Organization and structure of precipitation cloud systems. *Advances in Geophysics*, Vol. 24, Academic Press, 225–328.

——, J. D. Locatelli and P. V. Hobbs, 1976: Dynamics and cloud microphysics of the rainbands in an occluded frontal system. *J. Atmos. Sci.*, **35**, 1921–1936.

Johnson, R. H., 1976: The role of convective-scale precipitation downdrafts in cumulus and synoptic scale interactions. *J. Atmos. Sci.*, **33**, 1890–1910.

——, 1980: Diagnosis of convective and mesoscale motions during Phase III of GATE. *J. Atmos. Sci.*, **37**, 733–753.

Kuo, H. L., 1965: On formation and intensification of tropical cyclones through latent heat release by cumulus convection. *J. Atmos. Sci.*, **22**, 40–63.

——, 1974: Further studies of the parameterization of the influence of cumulus convection of large-scale flow. *J. Atmos. Sci.*, **31**, 1232–1240.

Kuo, Y.-H., and R. A. Anthes, 1984a: Mesoscale budgets of heat and moisture in a convective system over the central United States. *Mon. Wea. Rev.*, **112**, 1482–1497.

——, and ——, 1984b: Accuracy of diagnostic heat and moisture budgets using SESAME-79 field data as revealed by observing system simulation experiments. *Mon. Wea. Rev.*, **112**, 1465–1481.

Lee, C.-S., 1984: The bulk effects of cumulus momentum transport in tropical cyclones. *J. Atmos. Sci.*, **41**, 590–603.

Le Mone, M. A., and W. T. Pennell, 1976: The relationship of trade wind cumulus distribution to subcloud layer fluxes and structure. *Mon. Wea. Rev.*, **104**, 524–539.

Lindzen, R. S., 1981: Some remarks on cumulus parameterization. Rep. on NASA–GISS Workshop: Clouds in Climate: Modelling and Satellite Observational Studies, 42–51.

Lord, S. J., 1982: Interaction of a cumulus cloud ensemble with the large-scale environment. Part III: Semiprognostic test of Arakawa–Schubert cumulus parameterization. *J. Atmos. Sci.*, **39**, 88–103.

Louis, J.-F., M. Tiedtke and J.-F. Geleyn, 1982: A short history of the PBL parameterization of ECMWF. *ECMWF Workshop on Planetary Boundary Layer Parameterization*, Reading, U.K., 59–79. [Available from ECMWF, Shinfield Park, Reading, Berkshire, U.K.]

Nitta, T., 1975: Observational determination of cloud mass flux distributions. *J. Atmos. Sci.*, **32**, 73–91.

——, 1978: A diagnostic study of interaction of cumulus updrafts and downdrafts with large-scale motions in GATE. *J. Meteor. Soc. Japan*, **56**, 232–241.

Ogura, Y., and H.-R. Cho, 1973: Diagnostic determination of cumulus cloud populations from observed large-scale variables. *J. Atmos. Sci.*, **30**, 1276–1286.

——, and ——, 1974: On the interaction between the subcloud and cloud layers in tropical regions. *J. Atmos. Sci.*, **31**, 1850–1859.

Reed, R. J., and E. E. Recker, 1971: Structure and properties of synoptic-scale wave disturbances in the equatorial Western Pacific. *J. Atmos. Sci.*, **28**, 1117–1133.

——, and R. H. Johnson, 1974: The vorticity budget of synoptic-scale wave disturbances in the tropical Western Pacific. *J. Atmos. Sci.*, **31**, 1784–1790.

Riehl, H., T. C. Yeh, J. S. Malkus and N. E. La Seur, 1951: The North-East trade of the Pacific Ocean. *Quart. J. Roy. Meteor. Soc.*, **77**, 598–626.

Schneider, E. K., and R. S. Lindzen, 1976: A discussion of the parameterization of momentum exchange of cumulus convection. *J. Geophys. Res.*, **81**, 3158–3160.

Shapiro, L. F., and D. E. Stevens, 1980: Parameterization of convective effects on the momentum and vorticity budgets of synoptic-scale Atlantic tropical waves. *Mon. Wea. Rev.*, **108**, 1816–1826.

Simpson, J., 1971: On cumulus entrainment and one-dimensional models. *J. Atmos. Sci.*, **28**, 449–455.

——, and V. Wiggert, 1969: Models of precipitating cumulus towers. *Mon. Wea. Rev.*, **97**, 471–489.

Sui, C.-H., and M. Yanai, 1986: Cumulus ensemble effects on the large-scale vorticity and momentum fields of GATE. Part I: Observational evidence. *J. Atmos. Sci.*, **43**, 1618–1642.

Thompson, R. M., Jr., S. W. Payne, E. E. Recher and R. J. Reed, 1979: Structure and properties of synoptic scale wave disturbances in the intertropical convergence zone of the Eastern Atlantic. *J. Atmos. Sci.*, **36**, 53–72.

Thomson, S. L., and D. L. Hartmann, 1979: Cumulus friction: estimated influence on the tropical mean meridional circulation. *J. Atmos. Sci.*, **36**, 2022–2026.

Tiedtke, M., 1988: Parameterization of cumulus convection in large-scale models. *Physically-Based Modelling and Simulation of Climate and Climate Change*, M. Schlesinger, Ed. D. Reidel, 375–431.

——, W. A. Heckley and J. Slingo, 1988: Tropical forecasting at ECMWF: On the influence of physical parameterization on the mean structure of forecasts and analyses. *Quart. J. Roy. Meteor. Soc.*, **114**, 639–664.

Turner, J. S., 1963: The motion of buoyant elements in turbulent surroundings. *J. Fluid. Mech.*, **16**, 1–16.

Wagner, V., 1975: Relationships between the tropospheric circulation and energetic processes within the Hadley circulation over the Atlantic Ocean. Ber. Inst. Radiometeor. und Maritime Meteor. Universität Hamburg, No. 26, 83 pp.

Wexler, R., and D. Atlas, 1959: Precipitation generating cells. *J. Meteor.*, **16**, 327–332.

Yanai, M., S. Esbensen and J.-H. Chu, 1973: Determination of bulk properties of tropical cloud clusters from large-scale heat and moisture budgets. *J. Atmos. Sci.*, **30**, 611–627.

——, J.-H. Chu, T. E. Stark and T. Nitta, 1976: Response of deep and shallow tropical maritime cumuli to large-scale processes. *J. Atmos. Sci.*, **33**, 976–991.